National Aeronautics and
Space Administration

U.S. CENTER 2014 LIMA

Hyperwall Science Stories

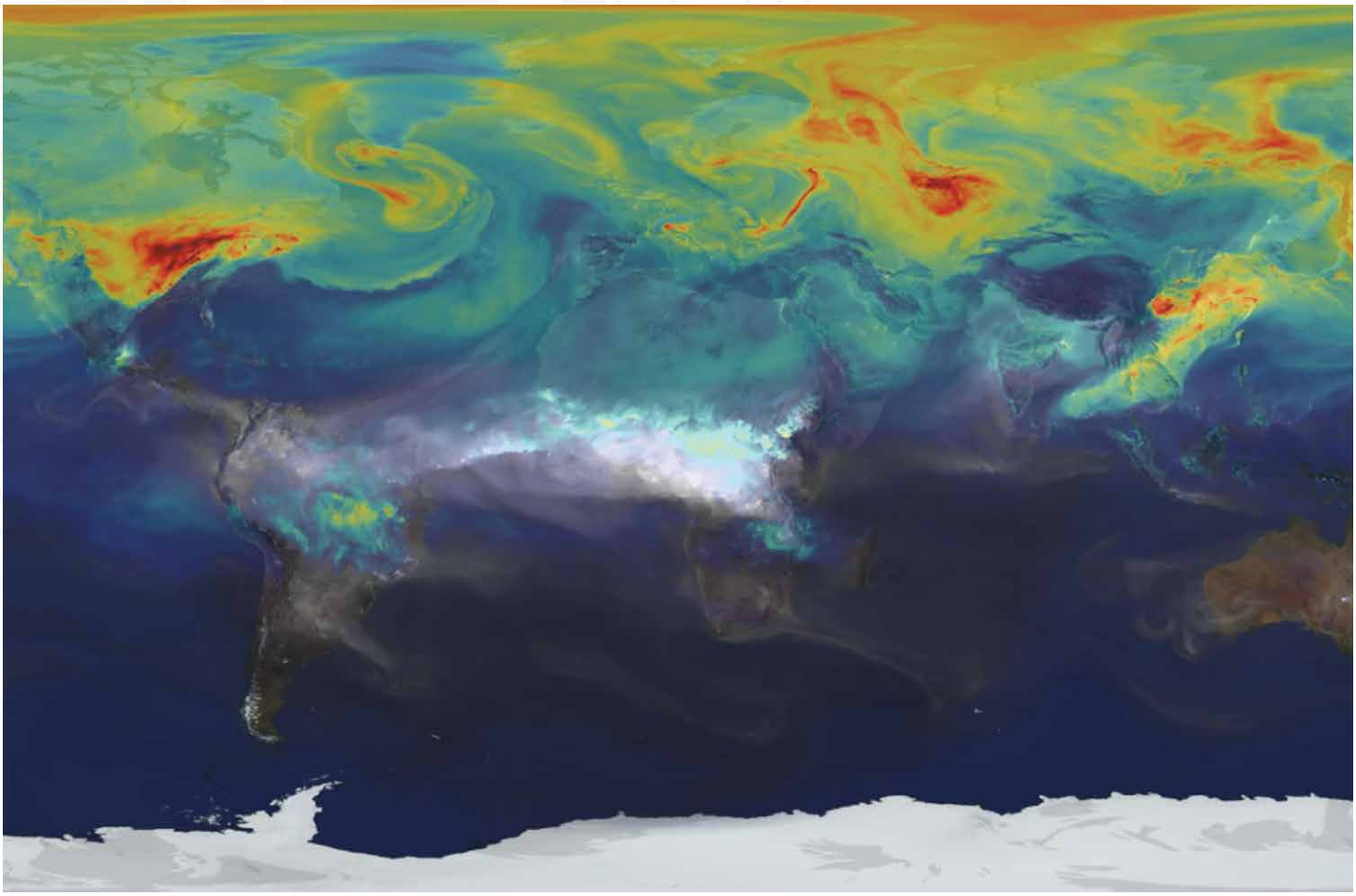

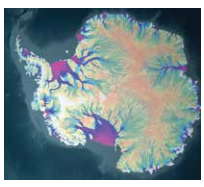

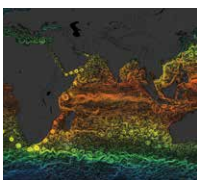

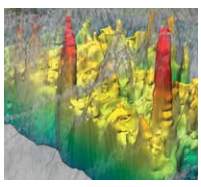
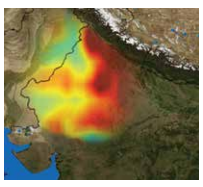
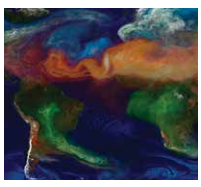

Hyperwall Stories are Available for Download as PowerPoint and Keynote Files at:

svs.gsfc.nasa.gov/hw

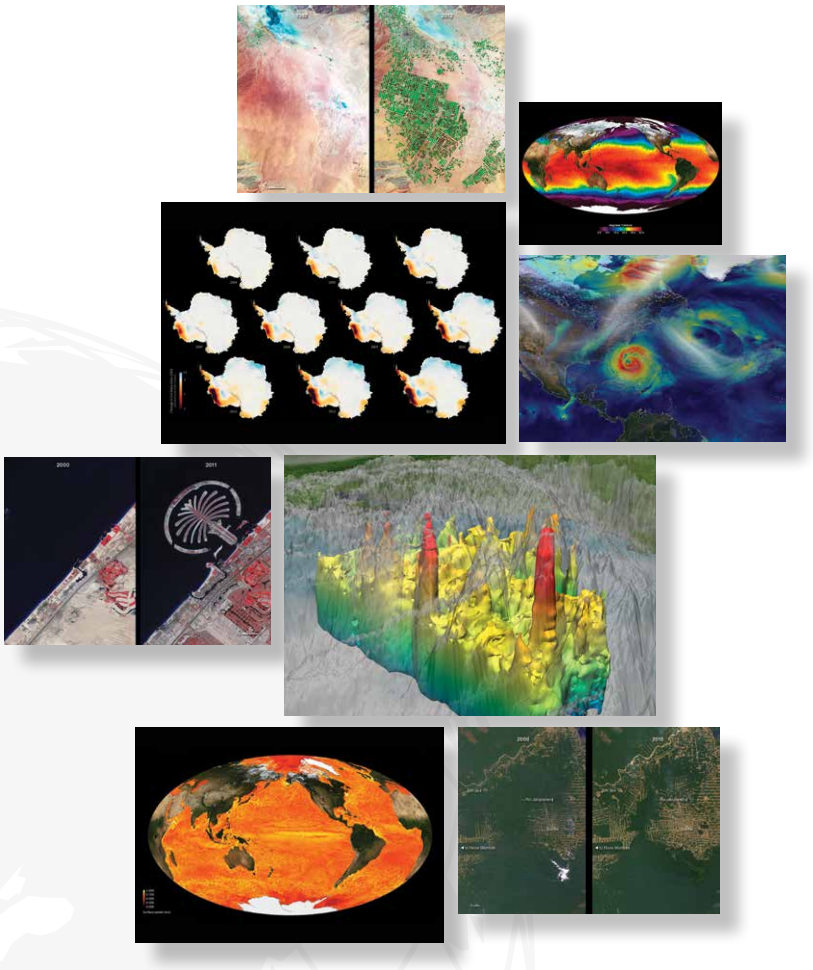

Table of Contents

Observing Earth from Space

Current Earth Science Satellite Missions

In order to study the Earth as a whole system and understand how it is changing, NASA develops and supports a large number of Earth observing missions. These missions provide Earth science researchers the necessary data to address key questions about global climate change.

Missions begin with a study phase during which the key science objectives of the mission are identified, and designs for spacecraft and instruments are analyzed. Following a successful study phase, missions enter a development phase whereby all aspects of the mission are developed and tested to insure it meets the mission objectives. Operating missions are those missions that are currently active and providing science data to researchers. Operating missions may be in their primary operational phase or in an extended operational phase. This graphic shows NASA's current fleet of Earth-observing satellite missions.

svs.gsfc.nasa.gov/goto?30065

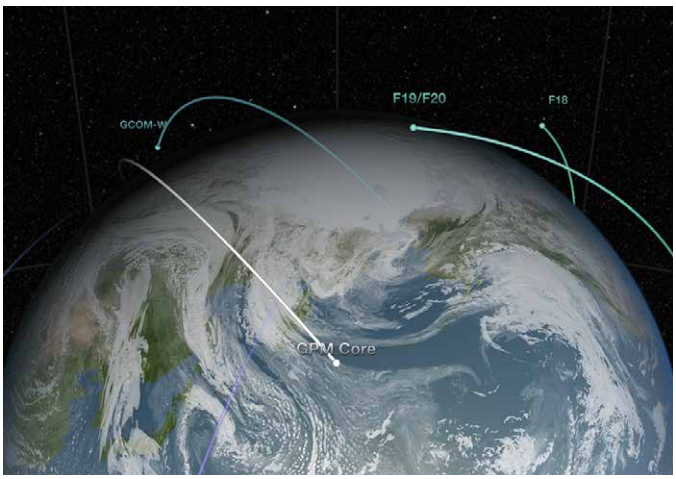

International Satellites Under One Umbrella

As the old adage goes: "when it rains, it pours." Unfortunately, scientists can't rely on a single satellite to provide global precipitation data. That's why NASA has teamed with the Japan Aerospace Exploration Agency and other international agencies to support the Global Precipitation Measurement (GPM) mission. GPM is an international satellite constellation with contributions from several international and domestic partners. Each satellite has its own purpose and mission, but the instruments aboard each satellite provide coverage of precipitation across the globe. The GPM Core Observatory satellite is equipped with two very important instruments that will provide three-dimensional images of rainfall and also extend our ability to measure light rain and snowfall. Ultimately, the GPM Core Observatory will unify measurements being taken by other instruments aboard other satellites and combine them into one global precipitation product.

svs.gsfc.nasa.gov/goto?3891

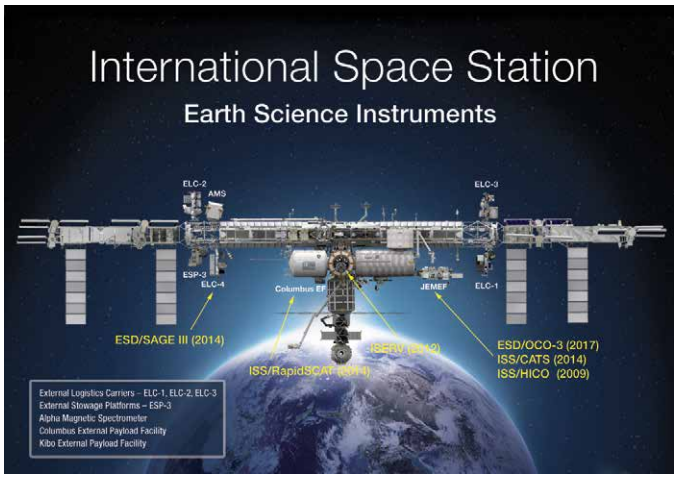

Future Earth Science Instruments on the International Space Station

The space station offers a unique vantage for observing the Earth's ecosystems with hands-on and automated equipment. These options enable astronauts to observe and explain what they witness in real time. Station crews can observe and collect camera images of events as they unfold and may also provide input to ground personnel programming the station's automated Earth-sensing systems. This flexibility is an advantage over sensors on unmanned spacecraft, especially when unexpected natural events, such as volcanic eruptions and earthquakes, occur.

A wide variety of Earth-observation payloads can be attached to the exposed facilities on the station's exterior; already, several instruments have been proposed by researchers from the partner countries. The station contributes to humanity by collecting data on the global climate, environmental change and natural hazards using its unique complement of crew-operated and automated Earth-observation payloads.

www.nasa.gov/mission_pages/station/research

Observing Earth from Space

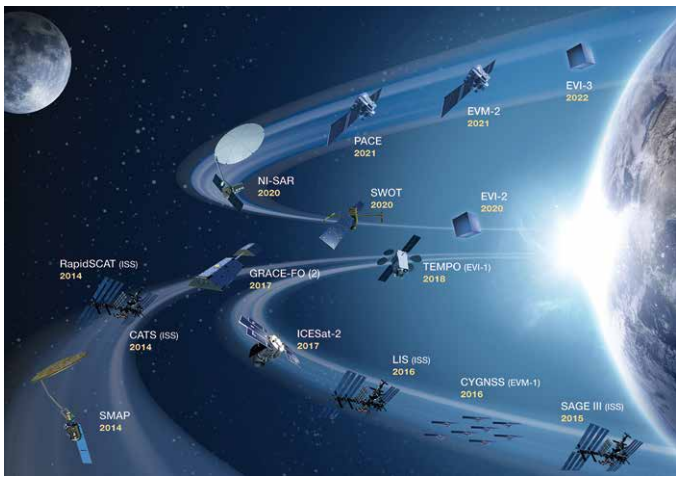

Future Earth Science Satellite Missions

To study the Earth as a whole system and understand how it is changing, NASA develops and supports a large number of Earth-observing missions. These missions provide Earth science researchers the necessary data to address key questions about global climate change.

This graphic shows NASA's Earth-observing missions planned to launch in the future. Missions begin with a study phase during which the key science objectives of the mission are identified, and designs for spacecraft and instruments are analyzed. Following a successful study phase, missions enter a development phase whereby all aspects of the mission are developed and tested to insure it meets the mission objectives.

svs.gsfc.nasa.gov/goto?30464

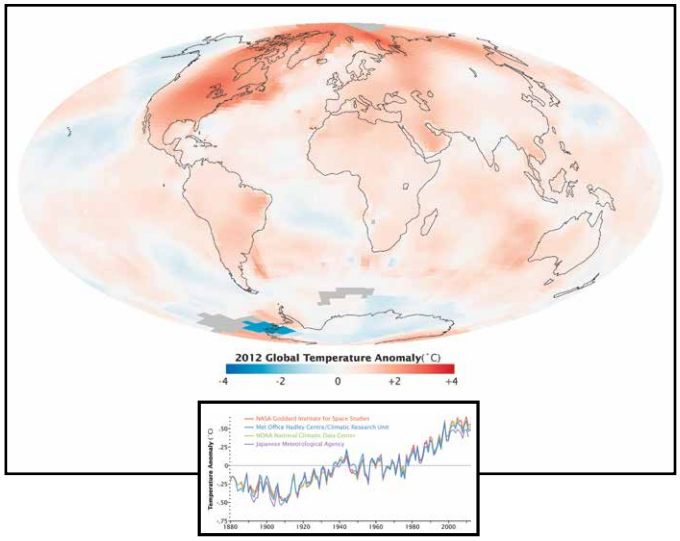

Long-Term Global Warming Trend

The world is getting warmer. This map shows global, annual temperature anomalies from 1880 to 2013 based on analysis conducted by NASA's Goddard Institute for Space Studies (GISS). Red and blue shades show how much warmer or cooler a given area was compared to an averaged base period from 1951 to 1980. The graph shows yearly, global GISS temperature anomaly data from 1880 to 2012. Though there are minor variations year to year, the general trend shows rapid warming in the past few decades, with the last decade being the warmest. To conduct its analysis, GISS uses publicly available data from approximately 6300 meteorological stations around the world; ship-based and satellite observations of sea surface temperature; and Antarctic research station measurements. Generally, warming is greater over land than over the oceans because water is slower to absorb and release heat. Warming may also differ within specific landmasses and ocean basins.

earthobservatory.nasa.gov/IOTD/view.php?id=80167

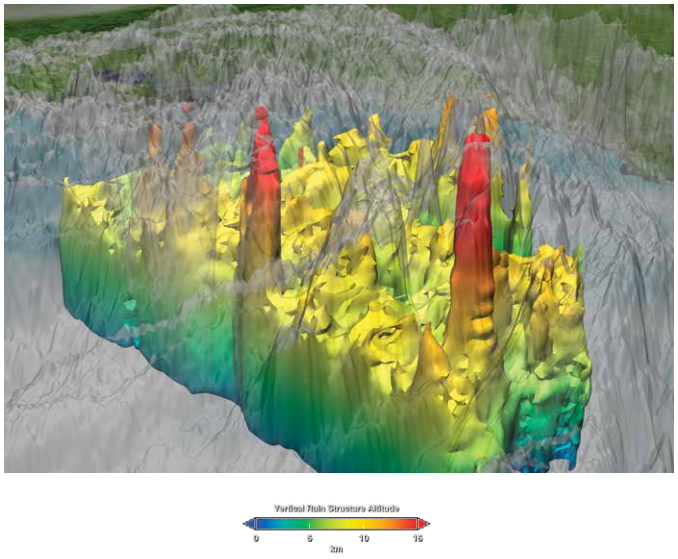

Hurricane Katrina Hot Towers

The Tropical Rainfall Measuring Mission (TRMM) spacecraft allowed us to look under Hurricane Katrina's clouds to see the rain structure on August 28, 2005. Just before Katrina strengthened into a Category 5 hurricane, TRMM observed tall cumulonimbus clouds, seen as red spikes, emerging from the storm's eyewall and rain bands. The spikes, named hot towers, are associated with tropical cyclone intensification because they emit tremendous amounts of heat that fuels the storm. The eyewall hot tower was approximately 10 miles (16 kilometers) tall.

Before TRMM, no dataset existed that could show globally and definitively the presence of these hot towers in cyclone systems. Now, scientists are combining observations from TRMM with supercomputing modeling power to shed light on the internal workings of hurricanes and how they intensify.

svs.gsfc.nasa.gov/goto?3253

Observing Earth from Space

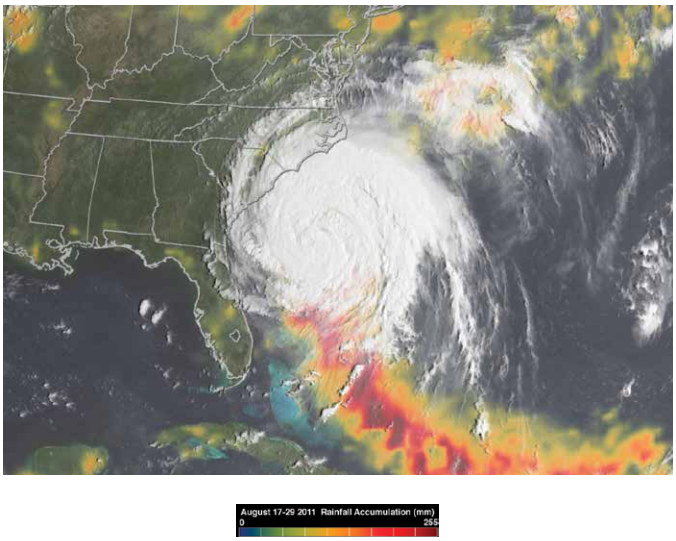

The Rainmaker

Each year hurricanes cause billions of dollars in damage across the United States. In August of 2011, Hurricane Irene roared up the densely populated East Coast dumping large amounts of rain on major cities. Floodwaters inundated roadways, communities, beaches, homes, and more from North Carolina to New England until the storm finally fizzled out over the Northern Atlantic. This visualization shows the spiraling storm as it trekked up the U.S. East Coast. Rainfall amounts were measured by the Microwave Imager onboard the Tropical Rainfall Measuring Mission (TRMM) satellite from August 17-29, 2011.

svs.gsfc.nasa.gov/goto?3852

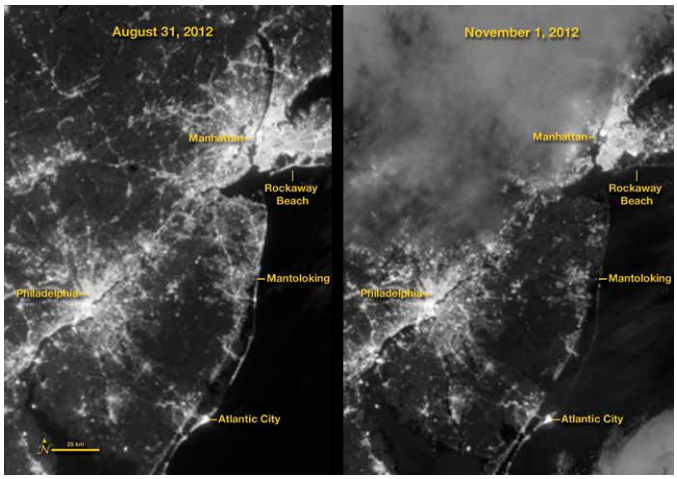

Blackout in New Jersey and New York

In the days following landfall of Hurricane Sandy, millions remained without power. This pair of images shows the difference in city lighting across New Jersey and New York before (August 31, 2012), when conditions were normal, and after (November 1, 2012) the storm. Both images were captured by the Visible Infrared Imaging Radiometer Suite (VIIRS) "day-night band" onboard the Suomi National Polar-orbiting Partnership satellite, which detects light in a range of wavelengths and uses filtering techniques to observe signals such as gas flares, city lights, and reflected moonlight. In Manhattan, the lower third of the island is dark on November 1, while Rockaway Beach, much of Long Island, and nearly all of central New Jersey are significantly dimmer. The barrier islands along the New Jersey coast, which are heavily developed with tourist businesses and year-round residents, are just barely visible in moonlight after the blackout.

earthobservatory.nasa.gov/IOTD/view.php?id=79589

A Changed Coastline in New Jersey

On October 29, 2012, Superstorm Sandy changed the lives of many living along the U.S. East Coast—especially along the shorelines of New Jersey, New York, and Connecticut. At landfall, heavy rains pelted states as far inland as Wisconsin and surging seawater washed away beaches and flooded streets, businesses, and homes.

These two images show a portion of the New Jersey coastal town of Mantoloking, just north of where the storm made landfall, before (March 18, 2007) and after (October 31, 2012) the storm. On the barrier island, entire blocks of houses along Route 35 (also called Ocean Boulevard) were damaged or completely washed away by the storm surge and wind. Fires raged in the town from natural gas lines that had ruptured and ignited. A new inlet was cut across the island, connected the Atlantic Ocean and the Jones Tide Pond.

earthobservatory.nasa.gov/IOTD/view.php?id=79622

Changes at Earth's Poles

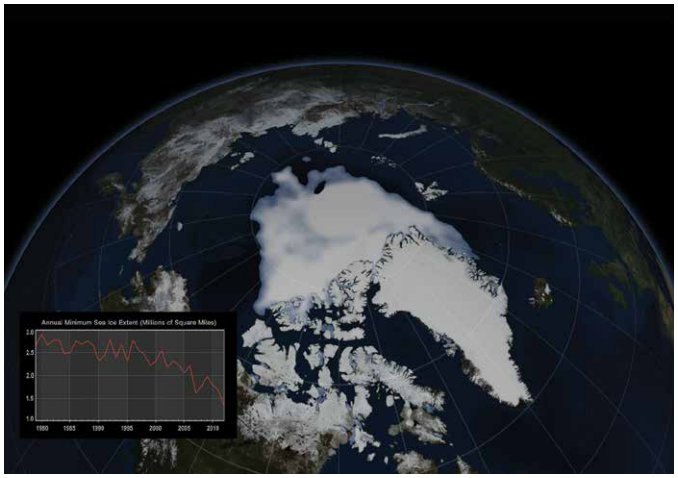

Annual Arctic Sea Ice Minimum Extents (1979-2013)

The Arctic Ocean is capped by frozen seawater, called sea ice, that melts during Northern Hemisphere spring and summer months before generally reaching its minimum extent in September each year. Since 1978, satellites have monitored sea ice growth and retreat, and they have detected an overall decline in Arctic sea ice. This visualization shows annual minimum Arctic sea ice extents from 1979 to 2013. The graph shows a downward trend in the minimum extents over this time period.

The satellite observations, from passive microwave sensors, are processed using algorithms developed by scientists at NASA. The data from the different sensors are carefully assembled to assure consistency throughout the 35-year record.

svs.gsfc.nasa.gov/goto?4004

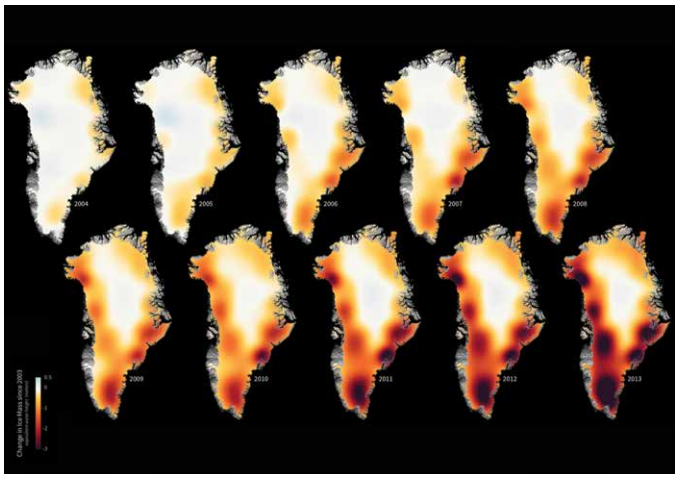

Greenland Ice Loss 2003-2013

The mass of the Greenland ice sheet has rapidly been declining over the last several years due to surface melting and iceberg calving. Research based on observations from NASA's twin Gravity Recovery and Climate Experiment (GRACE) satellites indicates that between 2003 and 2013, Greenland shed approximately 280 gigatons of ice per year, causing global sea level to rise by 0.8 millimeters per year. These GRACE images show changes in Greenland ice mass since 2003. Orange and red shades indicate areas that lost ice mass, while light blue shades indicate areas that gained ice mass. White indicates areas where there has been very little or no change in ice mass since 2003. In general, higher-elevation areas near the center of Greenland experienced little to no change, while lower-elevation and coastal areas experienced up to 3 meters of ice mass loss over a ten-year period. The largest mass decreases of up to 30 centimeters per year occurred over southeastern Greenland.

svs.gsfc.nasa.gov/goto?30478

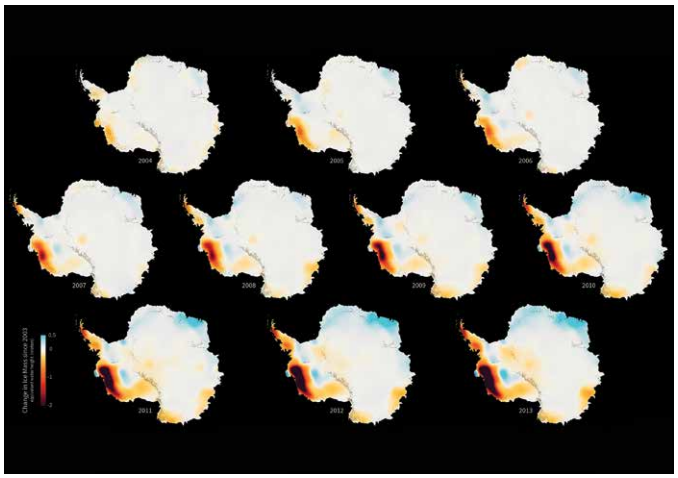

Antarctic Ice Loss 2003-2013

The mass of the Antarctic ice sheet has changed over the last several years. Research based on observations from NASA's twin Gravity Recovery and Climate Experiment (GRACE) satellites indicates that between 2003 and 2013, Antarctica shed approximately 90 gigatons of ice per year, causing global sea level to rise by 0.25 millimeters per year. These images, created with GRACE data, show changes in Antarctic ice mass since 2003. Orange and red shades indicate areas that lost ice mass, while light blue shades indicate areas that gained ice mass. White indicates areas where there has been very little or no change in ice mass since 2003. In general, areas near the center of Antarctica experienced small amounts of positive or negative change, while the West Antarctic Ice Sheet experienced a significant ice mass loss (dark red) over the ten-year period.

svs.gsfc.nasa.gov/goto?30492

Changes at Earth's Poles

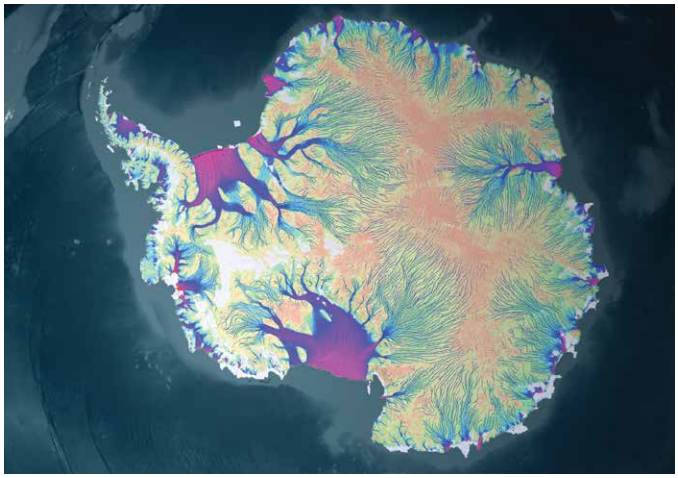

Antarctic Ice Flow

While Antarctica may appear stationary, it is actually a mosaic of moving ice sheets. Ice is naturally transported from the interior regions (where it accumulates from snowfall to the coastal regions) and is discharged to the ocean as tabular icebergs and ice-shelf melt water. This visualization shows the velocity of ice on Antarctica representing hundreds to thousands of years of motion. Ice velocity is color coded on a logarithmic scale with values varying from approximately 3 feet (~1 meter) per year (brown to green) to 2 miles (~3000 meters) per year (green to blue to red). These observations have vast implications for our understanding of the flow of ice sheets and how they might respond to climate change in the future and contribute to changes in global sea level.

svs.gsfc.nasa.gov/goto?3848

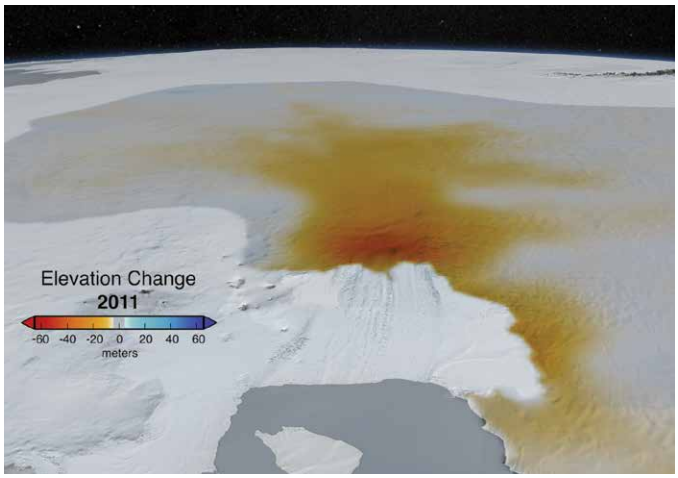

Pine Island Glacier Ice Flows and Elevation Change

The highly dynamic Pine Island Glacier, located on the West Antarctic Ice Sheet, is a large ice stream—a region of the ice sheet that moves faster than the surrounding ice. Scientists know that ice speeds in this area have increased dramatically from the late 1990s to present. As the ice accelerates, the ice upstream is stretched more vigorously, causing it to thin. This animation shows changes in ice velocity as well as elevation changes from 2002 to 2011. NASA-sponsored aircraft missions first measured the ice surface height in this region in 2002, followed by the Ice, Clouds, and Land Elevation Satellite (ICESat) between 2002 and 2009, and then the Operation IceBridge aircraft missions from 2009 to present. Integrating these altimetry sources allow scientists to estimate surface-height changes across the most important drainage glacier in the region. They have found that large and accelerating elevation changes extend inland from the coast on Pine Island Glacier.

svs.gsfc.nasa.gov/goto?3889

Bird's Eye View of a Crack in the Ice

On October 26, 2011, researchers flying in NASA's Operation IceBridge campaign made the first-ever detailed, airborne measurements of a major iceberg calving event that took place on Antarctica's Pine Island Glacier. The IceBridge team used the measurements collected during the 18-mile (~29-kilometer) flight path to map the crack in a way that allows us to fly through the icy canyon. The depth of the canyon ranged from 165 to 190 feet deep (~50-60 meters) with an average width of 240 feet (~73 meters). Radar measurements suggested the ice shelf is about 1640 feet (~500 meters) thick, with only 165 to 190 feet of that floating above water. The animation was created by draping aerial photographs from the Digital Mapping System over data from the Airborne Topographic Mapper.

svs.gsfc.nasa.gov/goto?10923

Changes at Earth's Poles

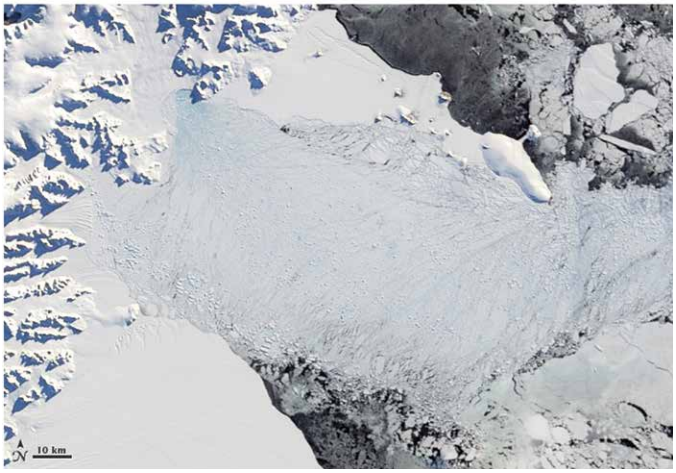

Collapse of the Larsen-B Ice Shelf

In the Southern Hemisphere summer of 2002, scientists monitoring daily satellite images of the Antarctic Peninsula watched almost the entire Larsen-B Ice Shelf splinter and collapse in just over one month. They had never witnessed such a large area—1250 square miles—disintegrate so rapidly. The collapse of the Larsen-B Ice Shelf was captured in this series of images between January 31 and April 13, 2002. At the start of the series, the ice shelf (left) is tattooed with pools of meltwater (blue). By February 17, the leading edge of the shelf had retreated about 6 miles. By March 7, the shelf had disintegrated into a blue-tinged mixture, or mélange, of slush and icebergs. The collapse appears to have been due to a series of warm summers on the Antarctic Peninsula, which culminated with an exceptionally warm summer in 2002. Warm ocean temperatures in the Weddell Sea that occurred during the same period might have caused thinning and melting underneath the ice shelf.

earthobservatory.nasa.gov/Features/WorldOfChange/larsenb.php

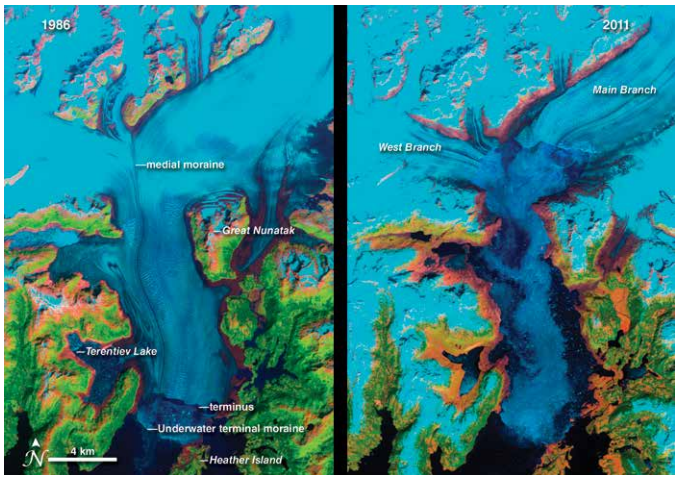

Columbia Glacier Alaska

The Columbia Glacier in Alaska is one of the most rapidly changing glaciers in the world. These false-color images show the glacier from 1986 to 2011. Snow and ice appears bright cyan, vegetation is green, clouds are white or light orange, and the open ocean is dark blue. Exposed bedrock is brown, while rocky debris on the glacier's surface is gray. By 2011, the terminus had retreated more than 20 kilometers (12 miles) to the north. Since the 1980s, the glacier has lost about half of its total thickness and volume. The ice losses are not exclusively tied to increasing air and water temperatures. Climate change may have given the glacier an initial nudge, but it has more to do with mechanical processes. In fact, when the glacier reaches the shoreline, its retreat will likely slow down. The more stable surface will cause the rate of calving to decline, making it possible for the glacier to start rebuilding a moraine and advancing once again.

earthobservatory.nasa.gov/Features/WorldOfChange/columbia_glacier.php

Earth's Ocean and Water Resources

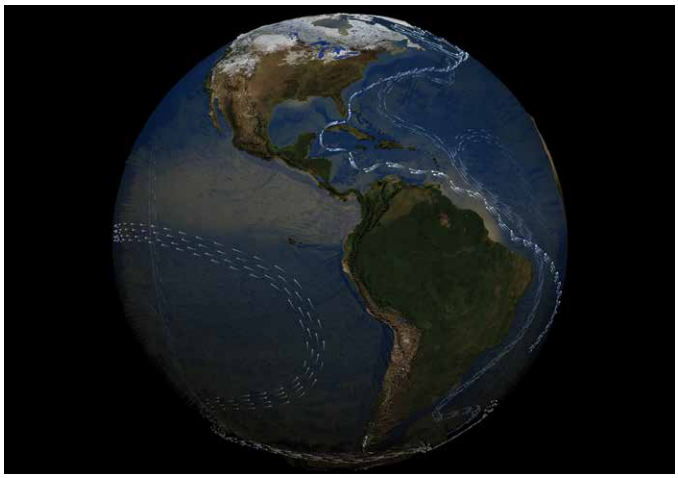

Earth's Circulatory System

In certain areas near the polar oceans, cooler surface water becomes saltier due to evaporation or sea ice formation and becomes dense enough to sink to the ocean depths. This "pumping" of surface water into the deep ocean forces water near the ocean floor to move horizontally (i.e., it circulates the water). The ocean's thermohaline circulation is driven by global density gradients such as these, caused by differences in ocean temperature—*thermo*—and salinity—*haline*. This animation shows one of the major regions of the thermohaline circulation—the North Atlantic Ocean around Greenland, Iceland, and the North Sea. It also shows the Antarctic Circumpolar Current, circling Antarctica. This circumpolar motion links the world's oceans and allows the deep water circulation from the Atlantic to rise in the Indian and Pacific Oceans, thereby closing the surface circulation loop.

svs.gsfc.nasa.gov/goto?3884

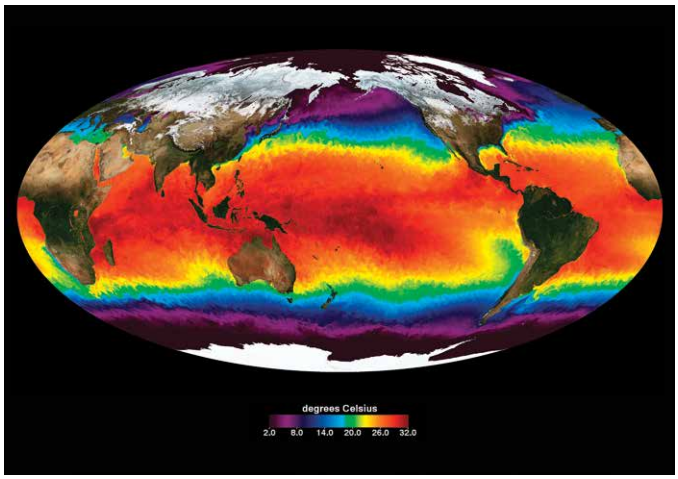

Sea-Surface Temperatures in Ultra-High Resolution

This animation from January 1, 2010 to December 31, 2011, shows global sea surface temperatures (SST) at 1-kilometer (~0.6 mile) resolution. Watch how Western Boundary Currents—fast-flowing currents that flow on the west side of ocean basins—such as the Gulf Stream and Kuroshio Current (near Japan) carry warm water from the tropics poleward. Additionally one can see the major upwelling areas (cooler temperatures) of the world's oceans associated with the California, Peruvian/Chilean, and Namibian/South African coasts. The Multi-scale Ultra-high Resolution (MUR) SST dataset combines data from the Advanced Very High Resolution Radiometer (AVHRR), Moderate Resolution Imaging Spectroradiometer (MODIS), and Advanced Microwave Scanning Radiometer for EOS (AMSR-E) instruments.

svs.gsfc.nasa.gov/goto?30008

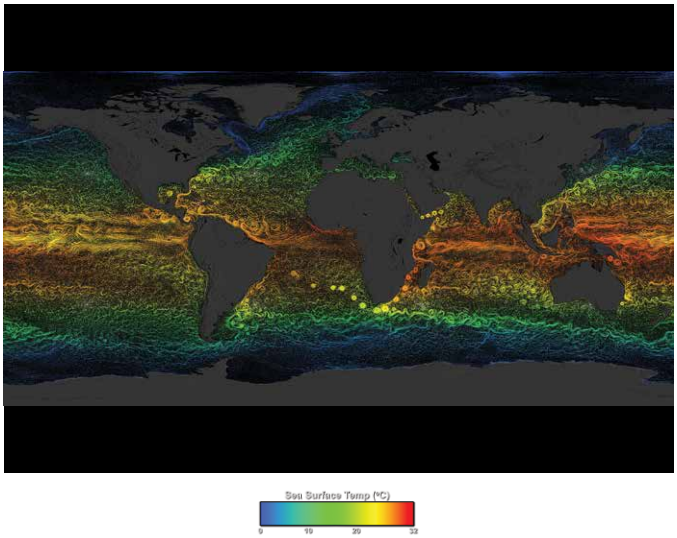

The Motions of the Ocean

The sun continually heats our planet, but the heating is unevenly distributed over Earth's surface. The tropics receive more energy than they emit and the polar regions emit more energy than they receive. Ocean water near the equator gets hotter and hotter while ocean water near the poles gets colder and colder. Nature won't stand for that kind of imbalance for very long. Its solution: the wind. Surface winds blow from areas of high pressure to low pressure, and help to steer ocean currents that transport heat in the ocean from the tropics to the poles. Scientists use model simulations like this one—produced by the Estimating the Circulation and Climate of the Ocean, Phase II (ECCO2)—to help resolve ocean eddies and other narrow-current systems that transport heat (and carbon) in Earth's ocean. In this animation, from March 25, 2007 to March 3, 2008, colors represent sea surface temperatures while the flow lines represent sea surface currents.

svs.gsfc.nasa.gov/goto?3912

Earth's Ocean and Water Resources

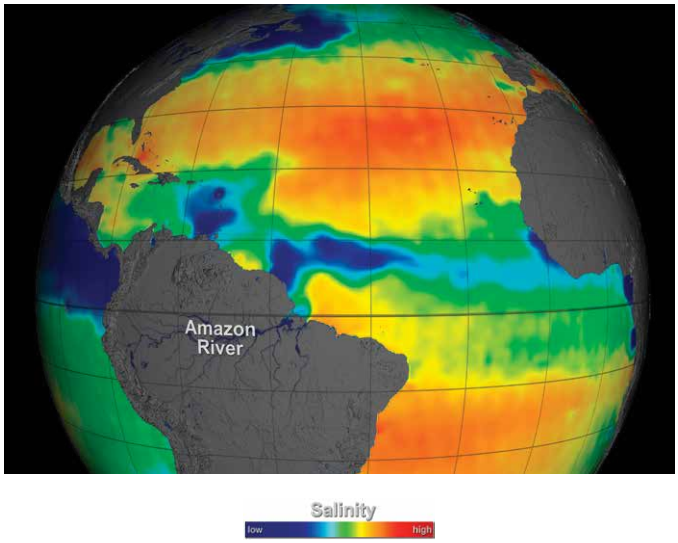

Sea-Surface Salinity Data from Aquarius in 2012

The Aquarius/SAC-D spacecraft is designed to measure global sea surface salinity. Aquarius is a collaboration between NASA and the Space Agency of Argentina. This visualization celebrates over a year of successful Aquarius observations. Sea surface salinity is shown at various locations around the globe highlighting the following: the Atlantic Ocean is generally much more salty than the Pacific; low salinity waters in the Eastern Equatorial Pacific are transported westward; high influxes of fresh water from the Amazon River basin can be clearly seen; low salinity waters are transported by the Labrador current to the south; and high influxes of fresh water from the Ganges River basin can be seen keeping the Eastern Indian Ocean lower salinity than the Western Indian Ocean. The range of time shown is December 2011 through December 2012. This visualization was generated based on version 2.0 of the Aquarius data products with all 3 scanning beams.

svs.gsfc.nasa.gov/goto?4045

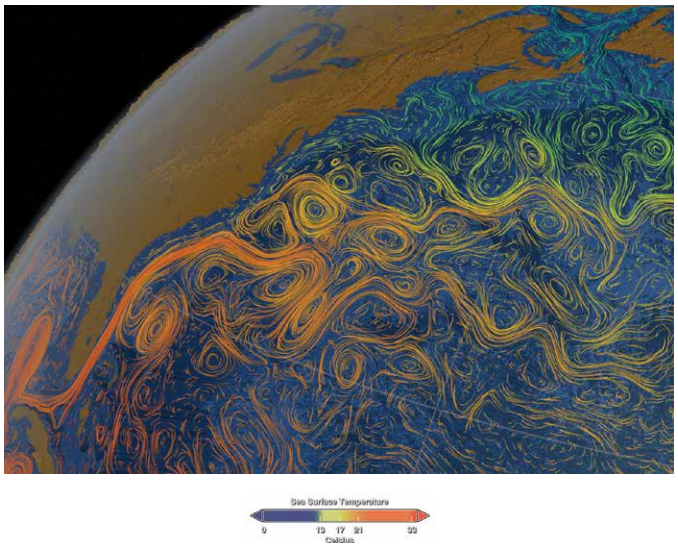

The Powerful Gulf Stream

The Gulf Stream is a powerful ocean current found in the Atlantic Ocean that transports warm water from the Gulf of Mexico along the South Atlantic Seaboard, subsequently influencing local weather patterns and climate. The current then turns northeastward crossing the Atlantic, where it exerts a warming influence on the climate of Western and Northern Europe, making these areas warmer then they would otherwise be. This visualization shows the warm-water Gulf Stream and its associated temperatures as it stretches across the Atlantic generating smaller currents and ocean eddies along the way. Model output from the Estimating the Circulation and Climate of the Ocean, Phase II (ECCO2) project were used to create this visualization. The project used a general circulation model to synthesize satellite and in situ data of the global ocean at resolutions that resolve ocean eddies and other narrow current systems that transport heat in the oceans.

svs.gsfc.nasa.gov/goto?3913

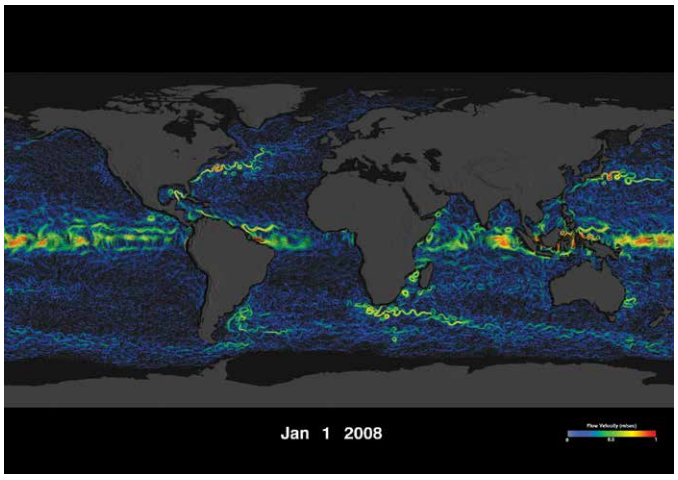

Speedy Ocean Currents

Ocean surface currents, mainly driven by prevailing winds, help transport heat and ocean nutrients around the world. This visualization shows surface ocean currents colored by velocities from January 1, 2008 to July 27, 2012. Blue shades indicate slow surface currents, while green and yellow shades indicate faster moving currents. Orange and red shades (the fastest currents) indicate velocities up to 1 meter (~3 feet) per second. Notice how fast-flowing currents such as those that flow on the west side of ocean basins—e.g., the Gulf Stream along the Eastern United States and Kuroshio Current near Japan—eventually disperse into slower, swirling eddies. This dataset—called the Ocean Surface Current Analysis Real-Time (OSCAR)—was derived from observed satellite altimetry and wind vector data. OSCAR data are produced by Earth & Space Research and distributed through the National Oceanic and Atmospheric Administration and NASA.

svs.gsfc.nasa.gov/goto?3958

Earth's Ocean and Water Resources

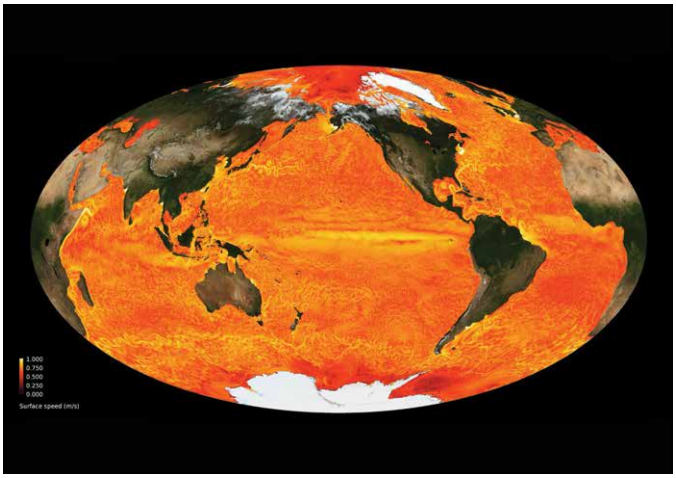

Simulated Sea Surface Speed

The speed of the ocean water near the surface, or sea surface speed, is influenced by many factors including surface winds, tides, diurnal cycles, atmospheric pressure forcings, as well as other dynamic and thermodynamic forces. Scientists use model simulations like this one—carried out by the ECCO group using the MIT general circulation model—to help resolve sea surface speeds in ultra-high resolution. Yellow shades represent relatively fast sea surface speeds, while red shades represent slower speeds. While winds near the surface of the ocean are the largest source of momentum for the ocean surface speed, the effects of several other oceanic characteristics are also visible, including the influence of tides, internal waves, and diurnal cycles. Several well known ocean features such as the Agulhas Current; the Gulf Steam; the north-flowing Kuroshio; and water flowing out from the mouth of the Amazon River are also visible.

svs.gsfc.nasa.gov/goto?30494

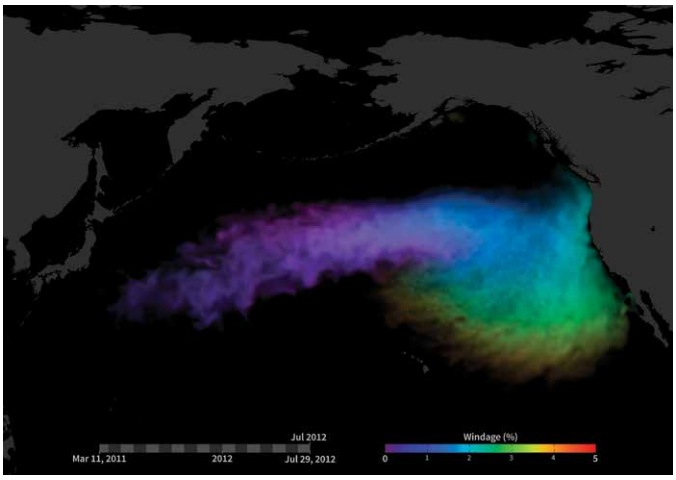

Wind-Blown Marine Debris from Japanese Tsunami

On Friday, March 11, 2011, a magnitude 9.0 undersea megathrust earthquake struck off the Pacific coast of Japan that generated tsunami waves that reached 40.5 meters high, traveling up to 10 kilometers inland in some areas (e.g., Sendai). The earthquake and resulting tsunami generated an estimated 24-25 million tons of rubble and debris in Japan. This simulation shows how winds near the ocean surface impacted the movement of marine debris as they moved across the Pacific from March 2011 to July 2012. The colors show the percentage of windage, or the amount of force (i.e., wind) created on an object by friction. Objects that float mostly above water are more impacted by the speed of the wind than the speed of the water; therefore, they have high windage values (orange/red shades). These objects move more quickly than objects that float mostly below water that are impacted more by the speed of the water and thus have low windage values (purple/blue shades).

svs.gsfc.nasa.gov/goto?30504

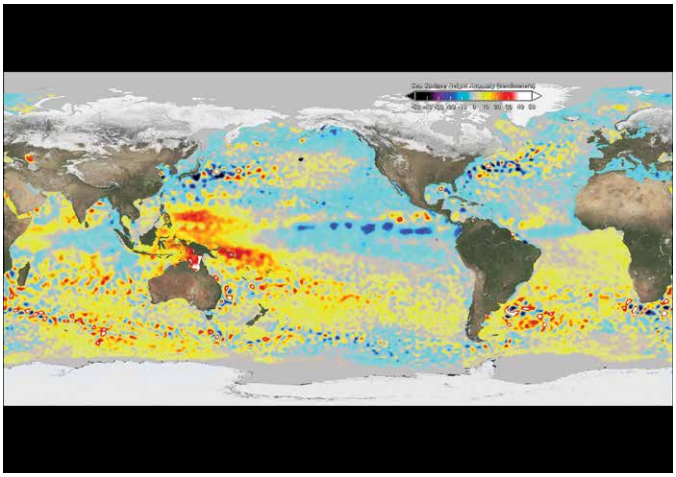

2009 El Niño & 2010 La Niña

Sea Surface Height Anomalies (SSHA) derived from Jason-2 satellite data show differences above and below normally observed sea surface heights. Large sustained above average areas (shown in orange and red) off the western coast of South America are an indicator of an El Niño event. In contrast, large sustained below average areas (shown in blue and violet) off the western South American coast are indicators of a La Niña event. This visualization shows the formation of an El Niño event towards the end of 2009 followed by a 2010 La Niña event.

svs.gsfc.nasa.gov/goto?3780

Earth's Ocean and Water Resources

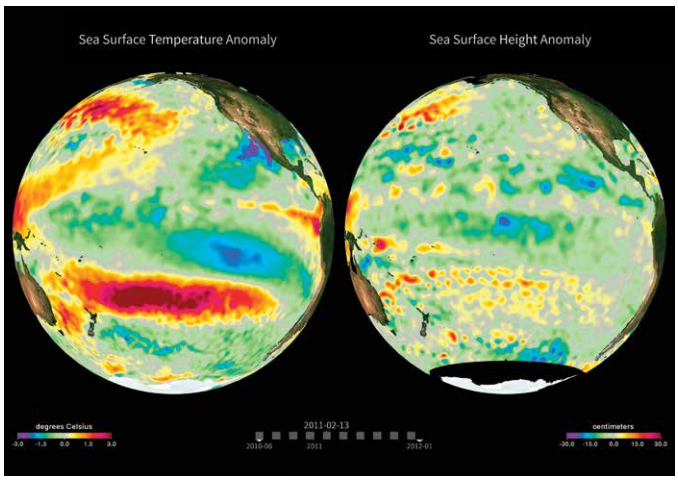

La Niña: Sea Surface Temperature and Height

This visualization from June 1, 2006 to December 31, 2011, illustrates the evolution of sea surface temperature (SST) and sea surface height (SSH) anomalies (relative to the respective normal state) associated with the 2010-2011 La Niña in the Pacific Ocean. SST and SSH anomalies reflect the heat content in the mixed layer (top 50 meters) and the upper ocean (top 150 meters), respectively. Typically, warm SST anomalies are often associated with high SSH anomalies, while cold SST anomalies are associated with low SSH anomalies. Therefore, they provide complimentary views of the oceanic signature of climate variability such as El Niño and La Niña. La Niña is the cooling phase of an interannual mode of climate variability called El Nino-Southern Oscillation. Initial cooling appeared in the eastern to central equatorial Pacific around June 2010 and grew into a relatively strong La Niña event in late 2010. The event persists beyond February 2011.

svs.gsfc.nasa.gov/goto?30489

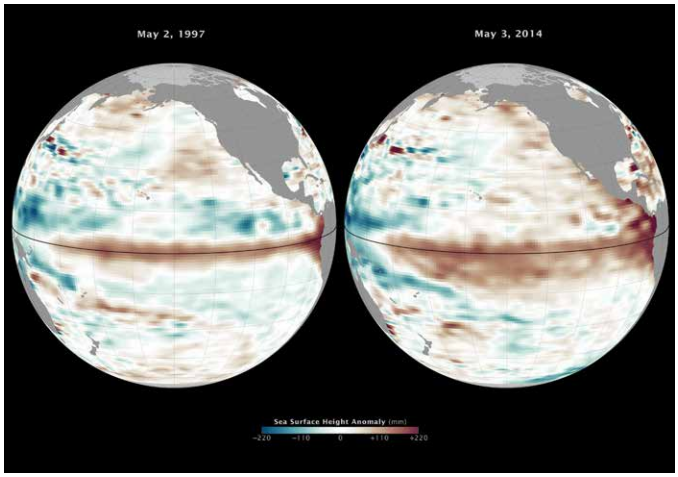

Is El Niño Developing?

Data from ocean-observing satellites and other ocean sensors indicate that El Niño conditions appear to be developing in the equatorial Pacific Ocean. Conditions in May 2014 bear some similarities to those of May 1997, a year that brought one of the most potent El Niño events of the twentieth century. As the ocean warms, the surface rises due to thermal expansion. Therefore, above-normal sea surface heights in the equatorial Pacific indicate El Niño conditions. These maps show the ten-day average of sea surface height centered on May 2, 1997 [*left*], and May 3, 2014 [*right*]. Reddish-brown shades indicate where the water is warmer and above normal sea level, while shades of blue-green show where sea level and temperatures are lower than average. Normal sea-level conditions appear in white. The 1997 map was assembled from data collected by the TOPEX/Poseidon satellite, while the 2014 data comes from the Ocean Surface Topography Mission/ Jason 2 satellite.

svs.gsfc.nasa.gov/goto?30509

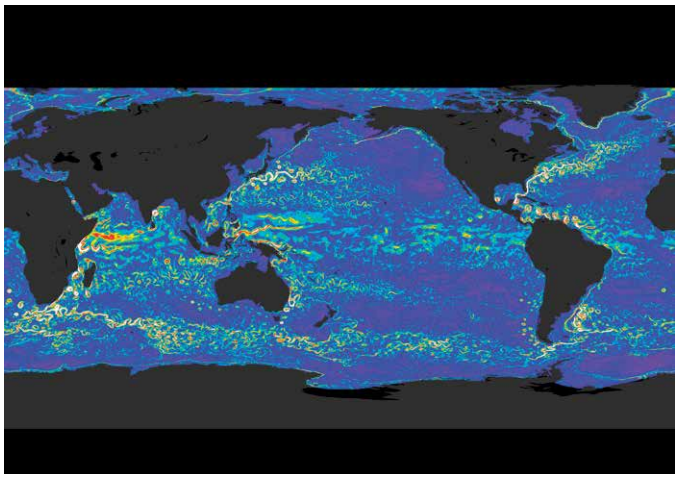

Altimetry: Past, Present, and Future

Launched in 1978, Seasat was the first NASA mission designed to observe the world's ocean. Seasat carried five major instruments, including a radar altimeter, indicating global sea surface height and the topography of the ocean surface. This visualization shows the progression of improved data resolution from satellite altimeters in the past, present, and future, beginning with 1.5-degree resolution data from Seasat and ending with 0.05-degree resolution data from NASA's SWOT mission, planned to launch in 2020. A single satellite (Geosat) provided 0.5-degree resolution data from 1986 to 1990, while numerous international satellite missions (ERS-1, TOPEX/Poseidon, ERS-2, Jason-1, Envisat, and Jason-2) have provided 0.25-degree resolution data from 1992 until now. SWOT (with 0.05-degree-resolution) will offer an unprecedented combination of spatial and temporal resolution while continuing and extending the ocean altimeter data record for years to come.

svs.gsfc.nasa.gov/goto?30500

Earth's Ocean and Water Resources

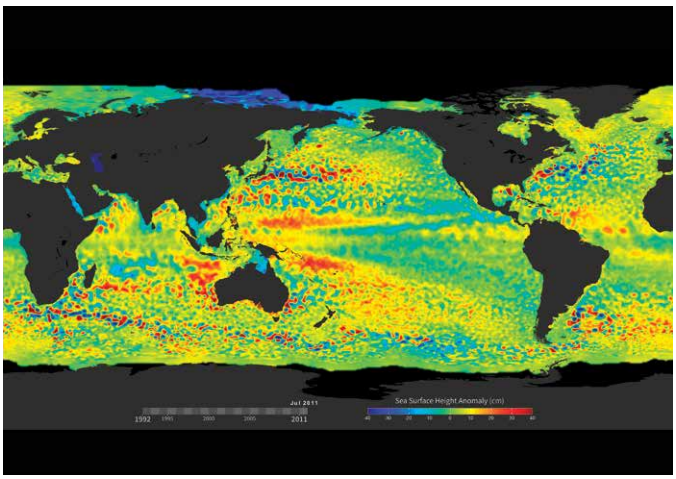

Sea Surface Height Anomalies, 1992-2011

Ocean tide gauges have been used for more than a century to measure sea surface height at specific locations around the globe. Today, scientists combine data from ocean tide gauges with global observations of sea surface height from satellite radar altimeters to detect patterns and monitor changes in ocean height. Currently, NASA's OSTM/Jason-2 mission—a continuation of the TOPEX/Poseidon and Jason missions—measures the height of the sea surface with an accuracy of about 3 centimeters (just over 1 inch) relative to the center of the Earth. These highly accurate measurements of the height of the sea surface (commonly called "sea level") are needed to provide long-term information about the world's ocean and its currents. In this visualization, sea surface height anomalies derived from ocean tide gauge data (before 1992) and satellite altimeter data (after 1992) show differences above and below normally observed sea surface heights from 1950 to 2009.

svs.gsfc.nasa.gov/goto?30502

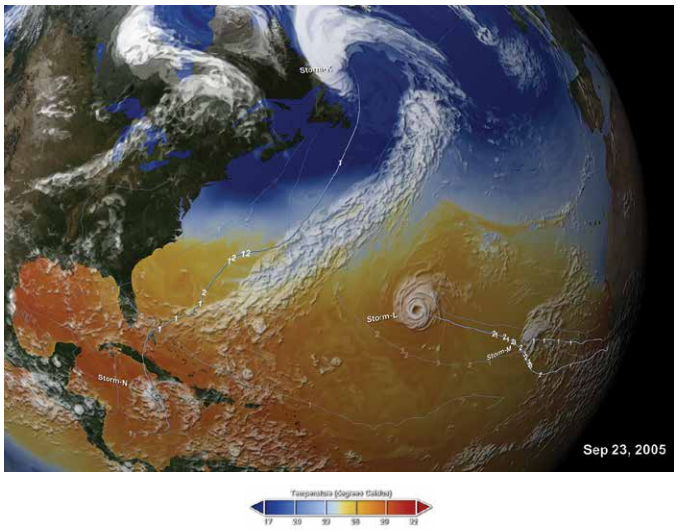

Modeling Hurricanes

The 2005 Atlantic Basin hurricane season was extremely active, producing a remarkable 27 storms in a six-month period. This visualization shows a Goddard Earth Observing System Model, Version 5 (GEOS-5) simulation of the very active hurricane season. Seeded only at the beginning of the run, the model shows 23 out of 27 storms—including Katrina. Considering this was an anomalous year, the model did a good job of simulating the large number of storms for that season. An innovative aspect of this global model is the ability to represent realistic hurricane intensities, including the six major hurricanes (i.e., Category 3 or higher on the Saffir-Simpson scale) that formed. Ocean colors ranging from blue to orange depict air temperature 2 meters (~6.6 feet) above sea level.

svs.gsfc.nasa.gov/goto?3887

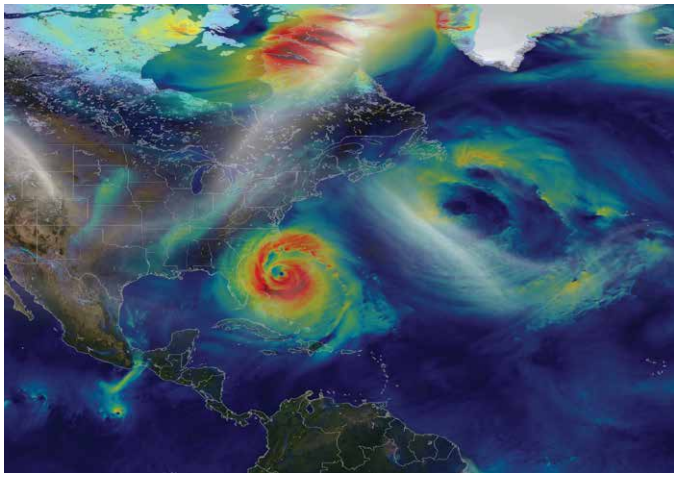

Hurricane Sandy Surface Winds

A rare combination of environmental conditions present during Hurricane Sandy's lifecycle gave rise to a storm of unforgettable magnitude—hence the nickname, Superstorm Sandy. This animation shows surface wind speeds from the GEOS-5 beginning September 1, 2012 with a 25-kilometer (~15.5-mile) model, preceding a higher-resolution 7-kilometer (~4.3-mile) global simulation with the GEOS-5 initialized on October 26, 2012. Surface wind speeds range from blue (10 miles per hour) to purple (80 miles per hour). The higher-resolution simulation depicts the strong onshore winds that continued to pummel New York and New Jersey even after landfall and the dramatic influence of the land surface slowing down Sandy's inland surface winds. Scientists can analyze the structure and lifecycle of severe storms like Sandy using the GEOS-5. What they learn can be incorporated into newer models, and result in even more accurate hurricane forecasts in the future.

svs.gsfc.nasa.gov/goto?30019

Earth's Ocean and Water Resources

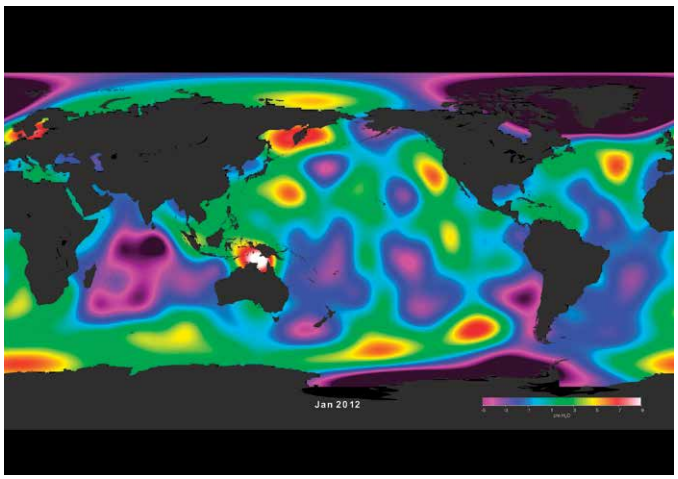

Ocean Bottom Pressure from GRACE

NASA's twin GRACE satellites, launched on March 17, 2002, have been making detailed measurements of Earth's gravity field from space and revolutionizing investigations about Earth's ocean, water reservoirs, large-scale solid Earth changes, and ice cover. To aid in the interpretation of gravity change over the oceans, the GRACE Tellus project provides ocean bottom pressure maps derived from the GRACE satellite data. Ocean bottom pressure is the sum of the mass of the atmosphere and ocean in a "cylinder" above the seafloor. This visualization shows monthly changes in ocean bottom pressure data obtained by the GRACE satellites from November 2002 to January 2012. Purple/blue shades indicate regions with relatively low ocean bottom pressure, while red/white shades indicate regions with relatively high ocean bottom pressure. Scientists use these data to observe and monitor changes in deep ocean currents, which transport water and energy.

svs.gsfc.nasa.gov/goto?30503

Sediment in the Gulf of Mexico

Clouds of sediment colored the Gulf of Mexico on November 10, 2009. Much of the color likely comes from re-suspended sediment dredged up from the sea floor in shallow waters. The sediment-colored water transitions to clearer dark blue near the edge of the continental shelf, where the water becomes deeper. The ocean turbulence that brought the sediment to the surface is readily evident in the textured waves and eddies within the tan and green waters. Tropical Storm Ida had come ashore over Alabama and Florida, immediately east of the area shown here, a few hours before the image was acquired. The storm's wind and waves may have churned up waters farther west. A second source of sediment is visible along the shore. Many rivers, including the Mississippi River, drain into the Gulf of Mexico in this region. The river plumes are dark brown that fade to tan and green as the sediment dissipates.

svs.gsfc.nasa.gov/goto?30287

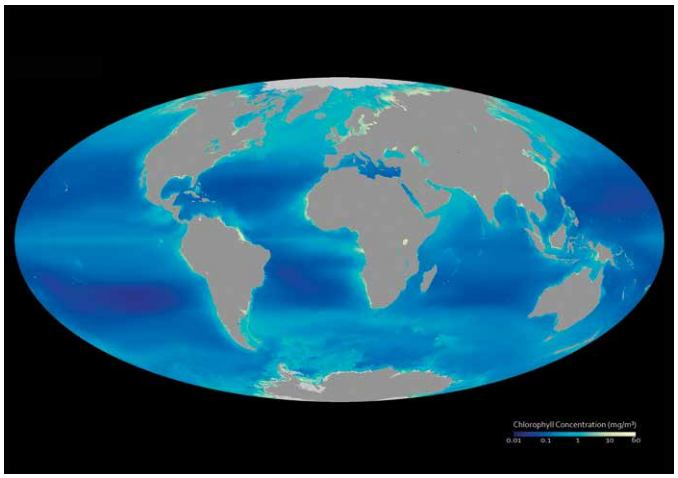

A Decade of Ocean Color

A decade of observations from the SeaWiFS satellite are represented in this image, which shows average chlorophyll concentrations in Earth's oceans from mid-September 1997 through the end of August 2007. Areas where plants thrive are light blue and yellow, while less productive regions are dark blue. In general, high chlorophyll corresponds with a high number of healthy plants. The global relationship between temperature and productivity was one that scientists first observed in SeaWiFS data. The places with the lowest chlorophyll concentrations are in the tropics, while the cold waters in the Arctic and Antarctic have high chlorophyll concentrations. What the image does not show is that the growth at the poles is seasonal. The plants only flourish during the spring and summer when there is sufficient light to fuel photosynthesis.

svs.gsfc.nasa.gov/goto?30289

Earth's Ocean and Water Resources

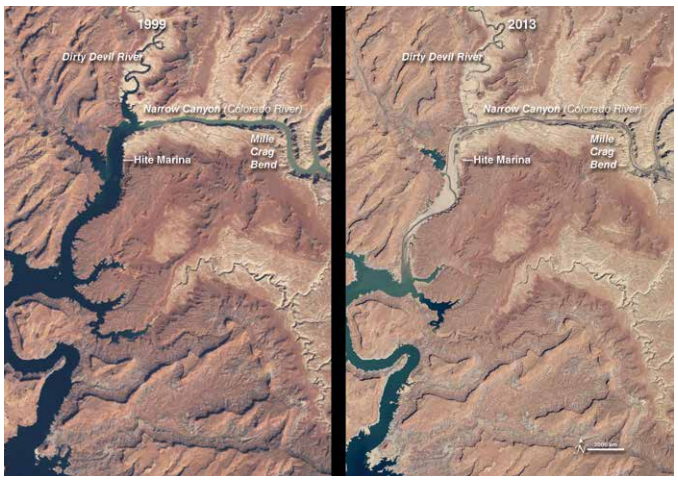

Water Level in Lake Powell

Among the dams on the Colorado River is the Glen Canyon Dam, which creates Lake Powell. This series of natural-color Landsat images shows the dramatic drop in Lake Powell's water level between 1999 and 2013 caused by prolonged drought and water withdrawals. At the beginning of the series, water levels were relatively high, and the water was a clear, dark blue. The sediment-filled river appeared green-brown. Dry conditions and falling water levels were unmistakable in the image from April 13, 2003, and again in early 2005 when water levels plummeted and the northwestern side branch of Lake Powell remained cut off from the rest of the reservoir. In the latter half of the decade the lake level began to rebound. Significant amounts of snowfall over the winter of 2010–2011 meant more water for the lake. Regional snowfall in the spring of 2012, on the other hand, was abnormally low, and inflow to Lake Powell did not begin to increase in May 2012 as it had in previous years. Daily water levels between October 2012 and May 2013 were consistently five or more feet below the previous four years. Droughts in this region are not unusual; however, global warming is expected to make droughts more severe in the future.

earthobservatory.nasa.gov/Features/WorldOfChange/lake_powell.php

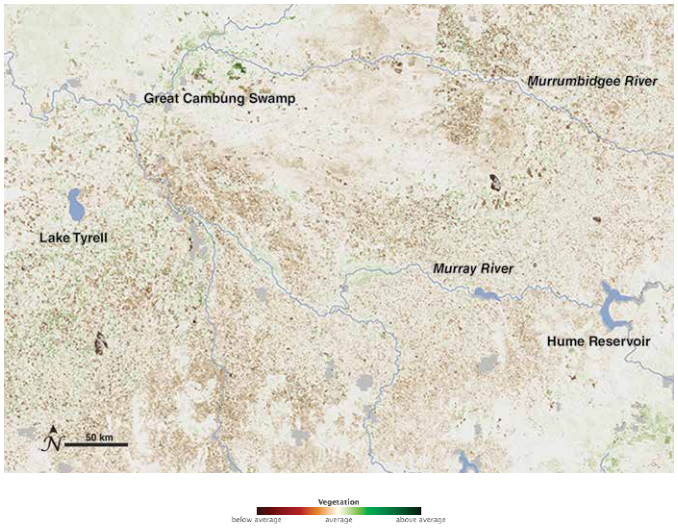

Drought Cycles in Australia

Drought is a frequent visitor in Australia. The Australian Bureau of Meteorology describes the typical rainfall over much of the continent as "not only low, but highly erratic." These satellite-based vegetation images document what farmers and ranchers have had to contend with over the past decade.

The images are centered on the agricultural areas near the Murray River—Australia's largest river—between Hume Reservoir and Lake Tyrrell. The series shows vegetation growing conditions for a 16-day period in the middle of September each year from 2000 through 2010 compared to the average mid-September conditions over the decade. Places where the amount and/or health of vegetation was above the decadal average are green, average areas are off-white, and places where vegetation growth was below average are brown.

earthobservatory.nasa.gov/Features/WorldOfChange/australia_ndvi.php

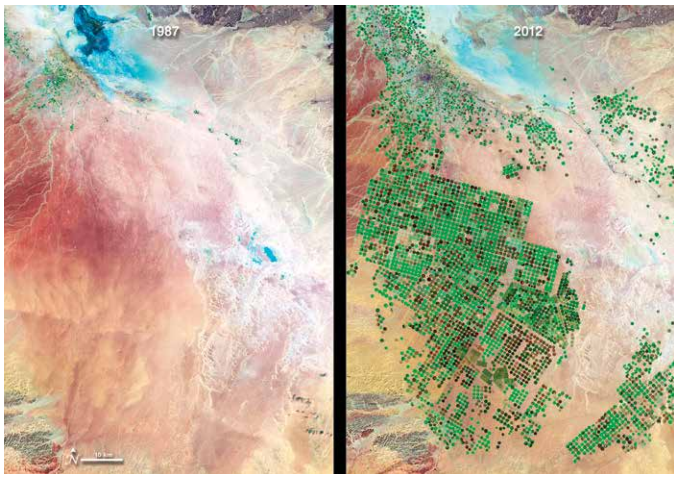

Thirst for Water: Crop Circles in the Desert

Over the past three decades, Saudi Arabia has been drilling for a resource more precious than oil. Engineers and farmers have tapped ancient reserves of water, dating back to the last Ice Age, to grow crops in the desert. This series of four false-color satellite images show the evolution of agricultural operations in the Wadi As-Sirhan Basin from 1987 to 2012. New vegetation appears bright green while dry vegetation or fallow fields appear rust colored. Dry, barren surfaces (mostly desert) are pink and yellow.

Saudi Arabians have reached this underground water source by drilling wells through sedimentary rock, as much as a kilometer beneath the desert sands. Rainfall averages just 100 to 200 millimeters per year and usually does not recharge the underground aquifers, making the groundwater a non-renewable source. Although no one knows how much water lies beneath the desert—estimates range from 252 to 870 cubic kilometers—hydrologists believe it will only be economical to pump it for about 50 years.

earthobservatory.nasa.gov/IOTD/view.php?id=77900

Earth's Ocean and Water Resources

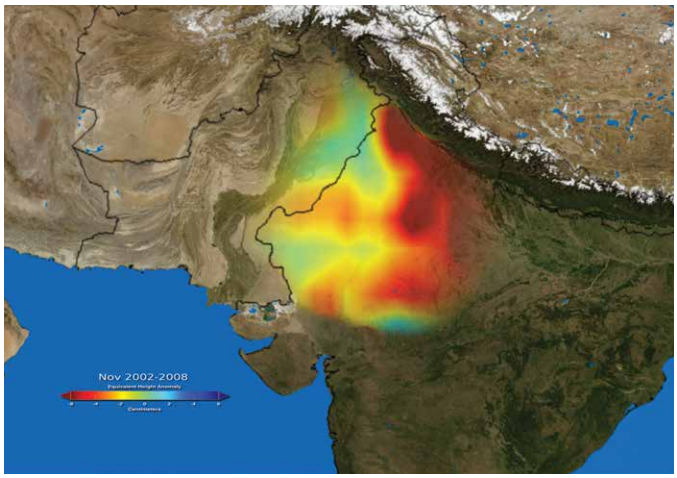

India Groundwater Depletion

Scientists using data from NASA's twin Gravity Recovery and Climate Experiment (GRACE) satellites have found that the groundwater beneath Northern India has been receding by as much as one foot per year over the past decade. After examining many environmental and climate factors, the team of hydrologists concluded that the loss is almost entirely due to human consumption. Groundwater comes from the natural percolation of precipitation and other surface waters down through Earth's soil and rock, accumulating in aquifers. When groundwater is pumped for irrigation or other uses, recharge to the original levels can take months or years.

More than 109 cubic km (26 cubic miles) of groundwater disappeared from the region's aquifers between 2002 and 2008--double the capacity of India's largest surface water reservoir, the Upper Wainganga, and triple that of Lake Mead, the largest manmade reservoir in the U.S. The animation shown here depicts the change in groundwater levels as measured each November between 2002 and 2008.

svs.gsfc.nasa.gov/goto?3623

Looking for Water Amidst the Heat

In Southern California irrigated farmland stretches north- and southward from the Salton Sea—an artificial inland sea in the desert. Blocks of square farmland appear in shades of green and tan in the natural-color image acquired on March 24, 2013 by the Operational Land Imager onboard the Landsat Data Continuity Mission—now renamed Landsat-8. On that same day, thermal measurements from the Thermal Infrared Sensor (grayscale image) show that the crops had different temperatures—specifically, cooler areas appear as dark shades, while warmer areas appear as bright shades. Dark pixels—representing cooler areas—in thermal images from TIRS help water managers determine where water is being used for irrigation. Plants cool down when they transpire, so the combination of water evaporating from the plants and the ground (i.e., evapotranspiration) lowers the temperature of the irrigated land. Scientists use these thermal measurements to calculate how much water agricultural fields are using.

earthobservatory.nasa.gov/IOTD/view.php?id=80958

Atmospheric Composition and Aerosols

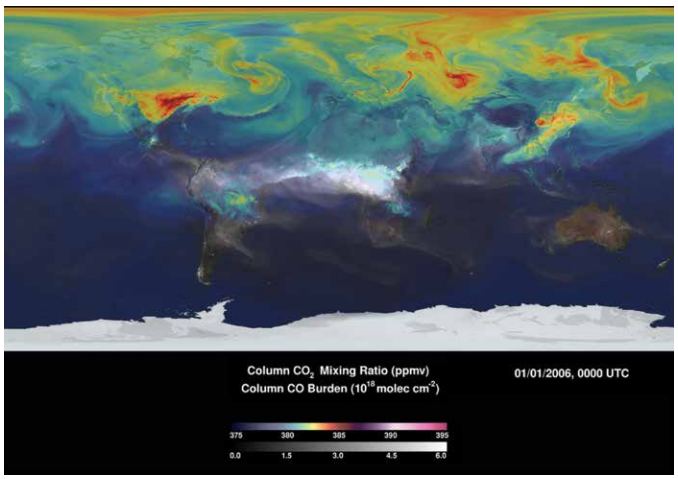

Simulated Atmospheric Carbon Concentrations

Carbon exists in many forms—e.g., carbon dioxide (CO_2), carbon monoxide (CO)—and continually cycles through Earth's atmosphere, ocean, and terrestrial ecosystems. This visualization, created using data from the 7-km GEOS-5 Nature Run model, shows average column concentrations of atmospheric CO_2 (colored shades) and CO (white shades underneath) from January 1, 2006 to December 31, 2006.

CO_2 variations are largely controlled by fossil fuel emissions and seasonal fluxes of carbon between the atmosphere and land biosphere. For example, dark red and pink shades represent regions where CO_2 concentrations are enhanced by carbon sources, mainly from human activities. During Northern Hemisphere spring and summer months, plants absorb a substantial amount of CO_2 through photosynthesis, thus removing CO_2 from the atmosphere. Atmospheric CO, a pollutant harmful to human health, is produced mainly from fossil fuel combustion and biomass burning. Here, high concentrations of CO (white) are mainly from fire activity in Africa, South America, and Australia. Scientists use model output data such as these to help answer important questions about Earth's climate.

svs.gsfc.nasa.gov/goto?30515

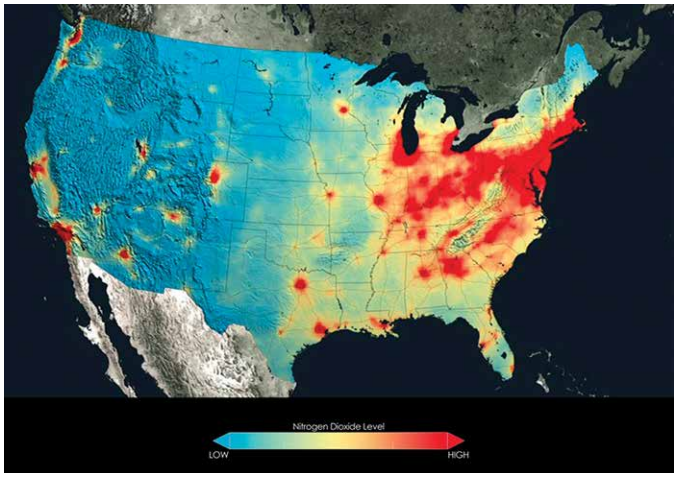

U.S. Air Quality Improvement

Anyone living in the U.S. for the past decade may have noticed a change in the air. The change is apparent in NASA satellite images that demonstrate the country's reduction of air pollution, or more specifically, nitrogen dioxide.

Nitrogen dioxide can impact the respiratory system, and it also contributes to the formation of other pollutants including ground-level ozone and particulates. The gas is produced primarily during the combustion of gasoline in vehicle engines and coal in power plants. Air pollution has decreased even though population and the number of cars on the roads have increased. The shift is the result of regulations, technology improvements and economic changes, scientists say.

This visualization shows tropospheric column concentrations of nitrogen dioxide across the U.S. as detected by the Ozone Monitoring Instrument on NASA's Aura satellite, averaged yearly from 2005-2011.

svs.gsfc.nasa.gov/goto?11579

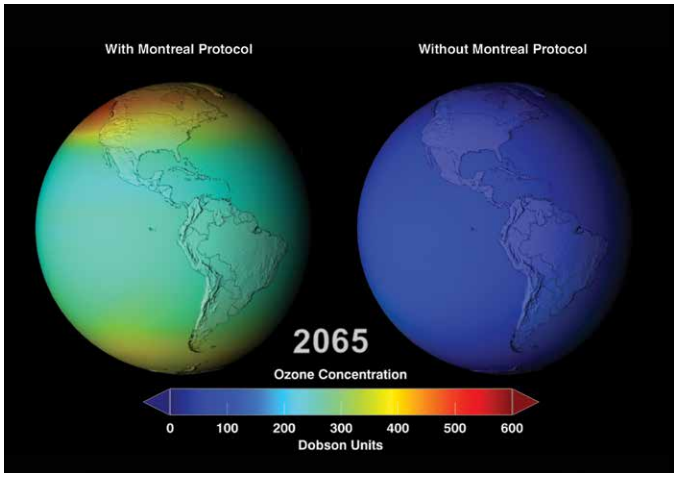

World Avoided

Led by NASA scientist Paul Newman, a team of atmospheric chemists, simulated "what might have been" if chlorofluorocarbons (CFCs) and similar ozone-depleting chemicals were not banned through the Montreal Protocol in the 1980s. The comprehensive model—including atmospheric chemical effects, wind changes, and solar radiation changes—simulated what would happen to global concentrations of stratospheric ozone if CFCs were continually added to the atmosphere.

This visualizations presents two cases: the world "With the Montreal Protocol," which assumes the current rate of emission, post-regulation, and the world "Without the Montreal Protocol," (the world avoided) where the rate of CFC emission into the atmosphere is assumed to be that of the period before regulation. Both cases were extrapolated to the year 2065.

svs.gsfc.nasa.gov/goto?3586

Atmospheric Composition and Aerosols

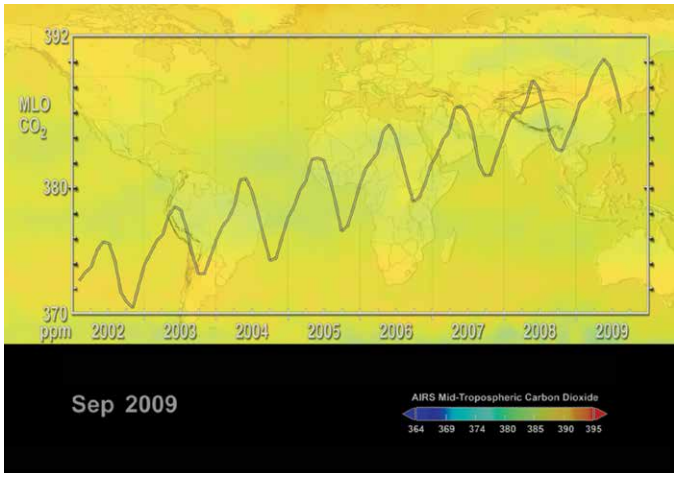

Global Carbon Dioxide with Mauna Loa Ground Obs

This visualization is a time-series of the global distribution and variation of the concentration of mid-tropospheric carbon dioxide observed by the Atmospheric Infrared Sounder (AIRS) on the NASA Aqua spacecraft. For comparison, it is overlain by a graph of the seasonal variation and interannual increase of carbon dioxide observed at the Mauna Loa, Hawaii observatory. The AIRS data show the average concentration (parts per million) over an altitude range of 3 km to 13 km, whereas the Mauna Loa data show the concentration at an altitude of 3.4 km and its annual increase at a rate of approximately 2 parts per million (ppm) per year.

svs.gsfc.nasa.gov/goto?3685

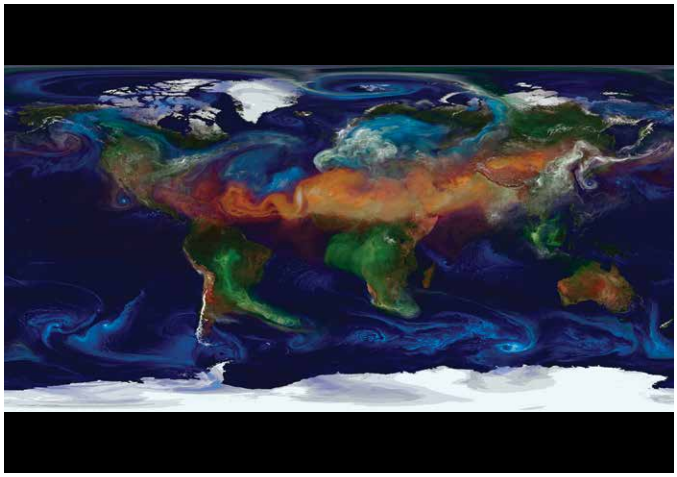

Around the World with Aerosols

Tiny solid and liquid particles suspended in the atmosphere are called aerosols. Windblown dust, sea salts, volcanic ash, smoke from wildfires, and pollution from factories are all examples of aerosols. Depending upon their size, type, and location, aerosols can either cool the surface, or warm it. They can help clouds to form, or they can inhibit cloud formation. And if inhaled, some aerosols can be harmful to people's health. To study aerosols, researchers from NASA's Global Modeling and Assimilation Office ran a simulation of the atmosphere that captured how winds transport aerosols around the world. The simulation shows sea salt and dust swirl inside cyclones, sulfates stream from volcanoes, and carbon burst from fires from May 2005 to May 2007, produced by the Goddard Earth Observing System Model Version 5, or GEOS-5. In general, dust appears in shades of orange, sea salt appears in shades of blue, sulfates appear white, and carbon appears in shades of green. Such simulations allow scientists to better understand how these tiny particulates travel in the atmosphere and influence weather and climate.

svs.gsfc.nasa.gov/goto?30017

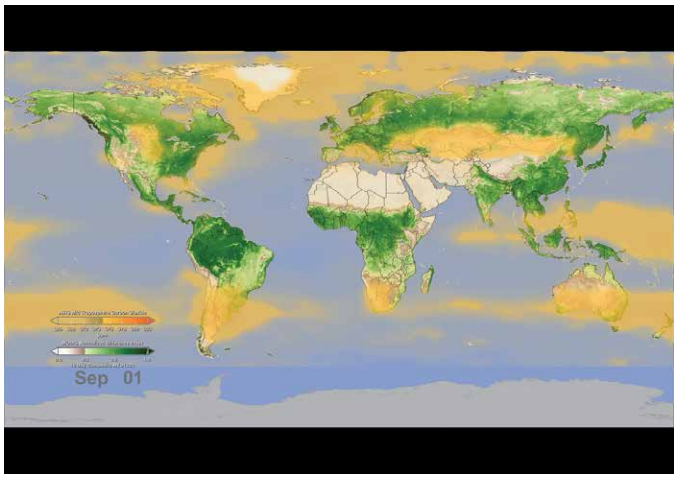

Watching the Earth Breathe

Trees and plants participate in the carbon cycle by "inhaling" carbon dioxide and converting it into organic plant matter as part of the process of photosynthesis, thus removing carbon dioxide from the middle part of Earth's lowest atmospheric layer—the troposphere. During Northern Hemisphere spring and summer for example, carbon dioxide in the troposphere decreases due to the large volume of new and growing vegetation, reaching a peak in late summer.

This animation shows daily average concentrations of mid-tropospheric carbon dioxide from January to December, shown in orange-yellow. The blooming effect of carbon dioxide follows a decrease in vegetation (green), as a result of seasonal changes (i.e., fall, winter). Data such as these give scientists an opportunity to better understand the relationship between carbon dioxide and the seasonal cycle of vegetation. The carbon dioxide values were made by averaging Atmospheric Infrared Sounder data from NASA's Aqua satellite, collected between 2003 and 2010 (e.g., the data used for January 1 is actually an average of eight years of AIRS carbon dioxide data taken each year on January 1). The vegetation values were made using data from the Moderate Resolution Imaging Spectroradiometer (MODIS) averaged from 2003 to 2006.

svs.gsfc.nasa.gov/goto?3947

Atmospheric Composition and Aerosols

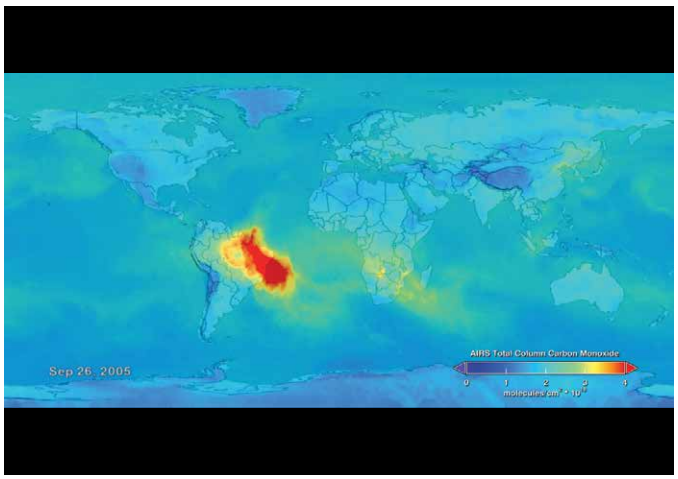

Beyond the Flames of Fire

Forest fires produce carbon monoxide (CO) along with copious amounts of other gases and particulate matter that subsequently change Earth's atmospheric composition. In the atmosphere, CO is short lived and therefore is detected close to its source. The CO seen here primarily comes from fires burning in the Amazon basin, with some additional contribution from fires in Southern Africa from August to September 2005. Red, orange, and yellow shades across South America, Africa, and the Atlantic Ocean points to high levels of CO. Notice the CO has transported from South America over the Atlantic Ocean to Africa and over the Indian Ocean to Australia. Instruments like the Atmospheric Infrared Sounder (AIRS)—aboard NASA's Aqua satellite—measure global atmospheric CO on a daily basis and help scientist better understand the impacts of CO on the atmosphere.

svs.gsfc.nasa.gov/goto?3882

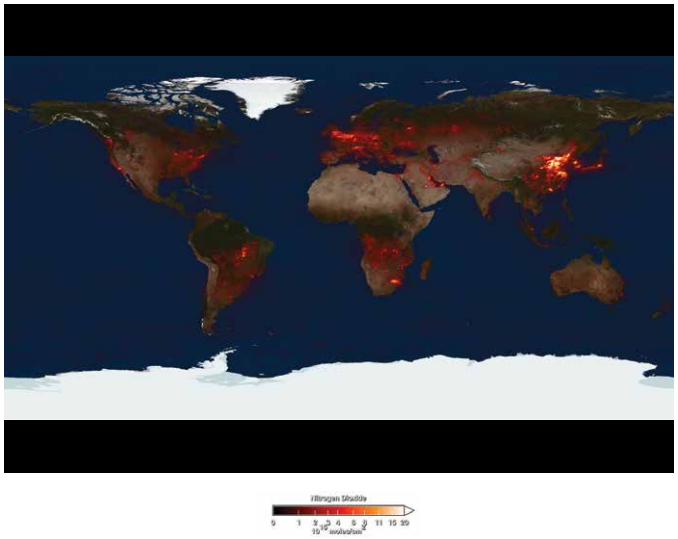

The Air We Breathe

Nitrogen Dioxide is a key component of urban air pollution. Most nitrogen dioxide is emitted by combustion (e.g., fossil fuels, wildfires). Major sources include industrial emissions, automobile traffic, forest and brush fires, microbiological soil emissions, lightning, and aircraft. More than half of the total nitrogen dioxide emissions are estimated to be anthropogenic, mainly from the burning of fossil fuels for energy production, transportation, and industrial activities. Nitrogen dioxide has a relatively short lifetime (about a day) and is therefore concentrated near its sources. This sequence of daily images from September 1, 2009 to August 31, 2010, shows the global perspective of tropospheric nitrogen dioxide as measured by the Ozone Measuring Instrument (OMI) flying aboard NASA's Aura spacecraft.

svs.gsfc.nasa.gov/goto?30014

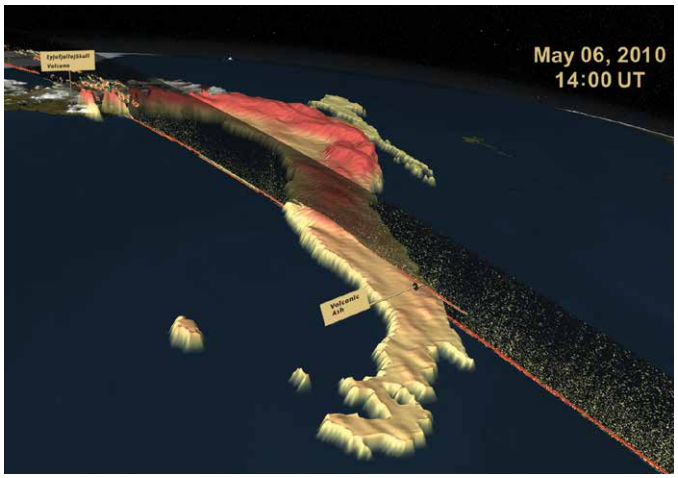

Iceland's Eyjafjallajökull Volcanic Ash Plume

A silica-rich plume composed of ash, smoke, and steam rose into the atmosphere over southern Iceland during the series of eruptions by Eyjafjallajökull volcano in spring 2010. Weary travelers were stranded at airports as air traffic across the Atlantic and over parts of Europe came to a halt. A European geostationary satellite, which orbits Earth above a single point, tracked the movement of the ash clouds as westerly winds carried them high above the ocean and toward northern Europe. Meanwhile, NASA's Cloud-Aerosol Lidar and Infrared Pathfinder Satellite Observation (CALIPSO) satellite measured the height and thickness of the material ejected into the atmosphere using its lidar instrument and infrared sensors. Together, the satellites created an unprecedented view of the eruption's aftermath. This visualization shows the movement and three-dimensional structure of the ash clouds released by Eyjafjallajökull volcano from May 6-8, 2010.

svs.gsfc.nasa.gov/goto?3783

Atmospheric Composition and Aerosols

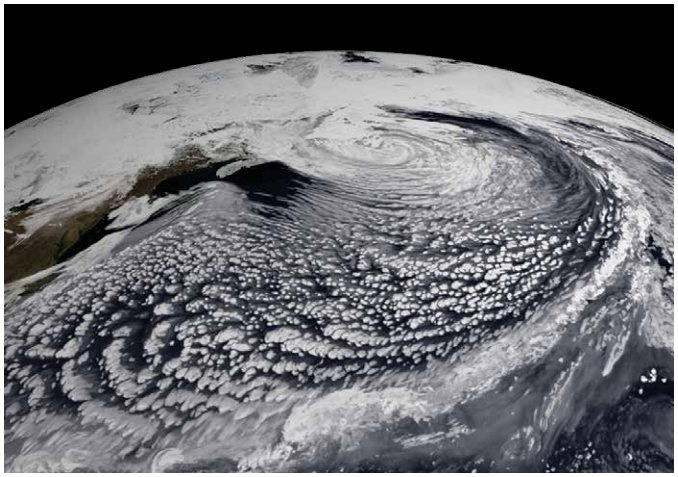

A Sea of Clouds

Earth's atmosphere is a fluid system not unlike our oceans, and both continuously work together to transport water around our planet. This visualization shows clouds from a simulation using the Goddard Earth Observing System Model, Version 5 (GEOS-5) for January 2, 2009. The sea of white appears to flow effortlessly above Earth's surface. Atmospheric winds steer the clouds in our atmosphere just as they steer the surface currents in our oceans, all the while exchanging water. Since there is only one day of simulation data, the sequence of clouds repeats several times. The white flash indicates the sequence is about to repeat. The simulation ran at 3.5 kilometers (~2 miles) per grid cell. The results were written out at 10-minute intervals.

svs.gsfc.nasa.gov/goto?3722

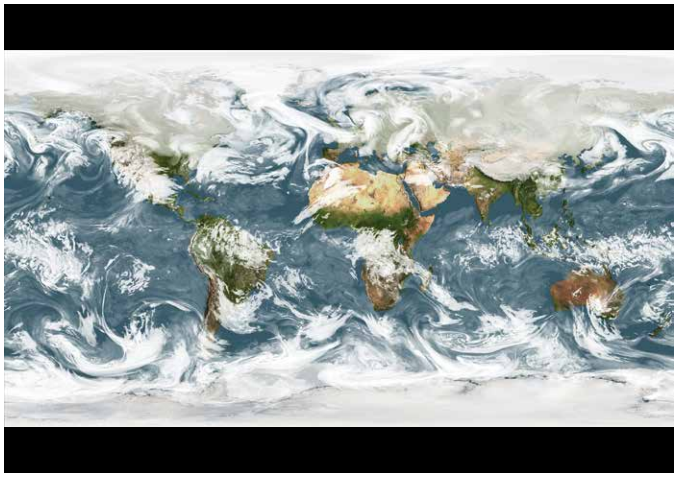

What's Up with Clouds?

From space, streaks of white clouds can be seen swirling across Earth's surface. If you stare long enough, you'll notice distinct patterns in the direction clouds move at certain latitudes. These patterns are a result of tropical regions receiving more energy than they emit and the polar regions emitting more energy than they receive. This latitudinal heat imbalance drives atmospheric circulation and subsequently causes weather. In this visualization, the intertropical convergence zone (ITCZ) is visible as a narrow band of clouds along the equator. Above and below the ITCZ, open cell cumulous clouds propagate westward. Most striking are the large swirls moving eastward located between 30–60° latitude, often referred to as mid-latitude cyclones.

The visualization shows a simulation of clouds from February 2-22, 2010, using the Goddard Earth Observing System Model, Version 5 (GEOS-5).

svs.gsfc.nasa.gov/goto?3723

Forests and Biodiversity

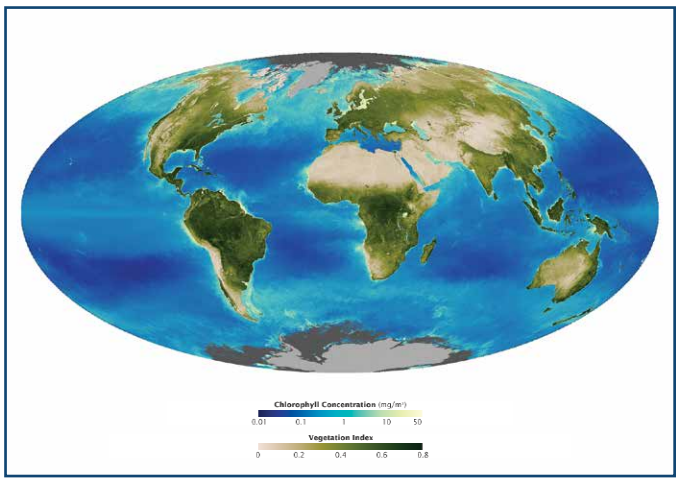

Global Biosphere

Turbulent storms churn the ocean in winter, adding nutrients to sunlit waters near the surface. This sparks a feeding frenzy each spring that gives rise to massive blooms of phytoplankton. Tiny green molecules found inside these microscopic plants harvest vital energy from sunlight through photosynthesis. The natural pigments, called chlorophyll, allow phytoplankton to thrive in Earth's oceans and enable scientists to monitor blooms from space. Satellites reveal the location and abundance of phytoplankton by detecting the amount of chlorophyll present in coastal and open waters. This visualization shows average 8-day chlorophyll concentrations observed by the SeaWiFS instrument from 1997-2003. On land, areas of high plant life are shown in dark green, while areas of low plant life are shown in tan. In the ocean, areas of high phytoplankton are shown in red, and areas of lowest phytoplankton are shown in blue and purple.

earthobservatory.nasa.gov/Features/WorldOfChange/biosphere.php

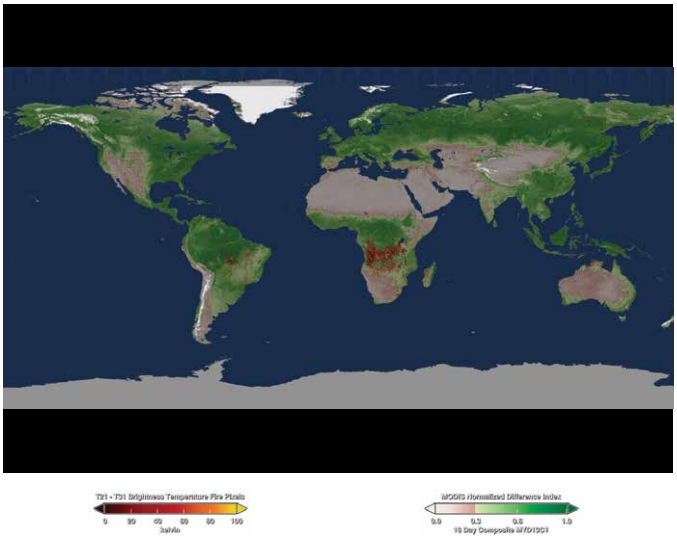

Global Fire Map

Fires can take place just about anywhere on the planet, but some locales seem more prone to fires than others. Observations from space have shown that approximately 70% of the world's fires occur in Africa alone.

This visualization shows fires across the globe between July 2002 and July 2011, and includes vegetation and snow cover data to show how fires respond to seasonal change. Fires can result from either natural processes, such as ignition by lighting strikes; or human activity, such as burning vegetation for agricultural purposes. As an example, almost all of the fires in the Amazon are the direct result of human activity, including slash-and-burn agricultural techniques. Instruments such as the Moderate Resolution Imaging Spectroradiometer (MODIS) onboard NASA's Aqua and Terra satellites detect fires from space.

svs.gsfc.nasa.gov/goto?3868

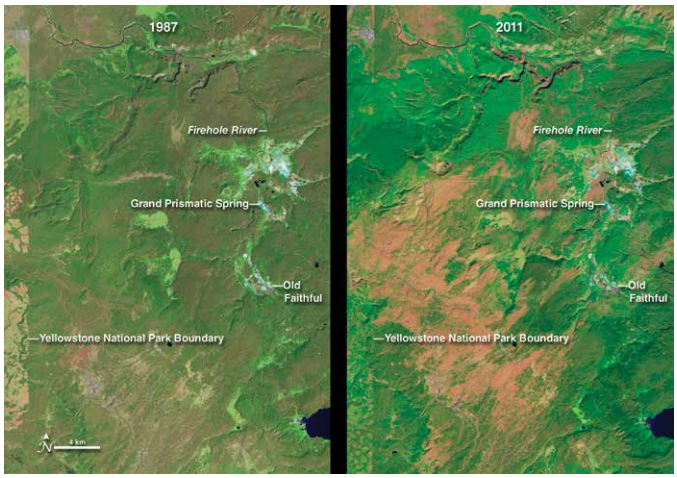

Burn Recovery in Yellowstone

In the summer of 1988, lightning- and human-ignited fires consumed vast stretches of Yellowstone National Park. By the time the first snowfall extinguished the last flames in September, 793,000 of the park's 2,221,800 acres had burned.

This series of images from 1987 to 2011, shows the burn scars left in the wake of the western Yellowstone fires and the slow recovery in the years that followed. Taken by Landsat-5, the images were made with a combination of visible and infrared light (green, short-wave infrared, and near infrared) to highlight the burned area and changes in vegetation. In the years that follow, the burn scar fades progressively. On the ground, grasses and wildflowers sprung up from the ashes and tiny pine trees took root and began to grow. Though changes did occur between 1988 and 2010, recovery has been slow. In 2010, the burned area is still clearly discernible.

earthobservatory.nasa.gov/Features/WorldOfChange/yellowstone.php

Forests and Biodiversity

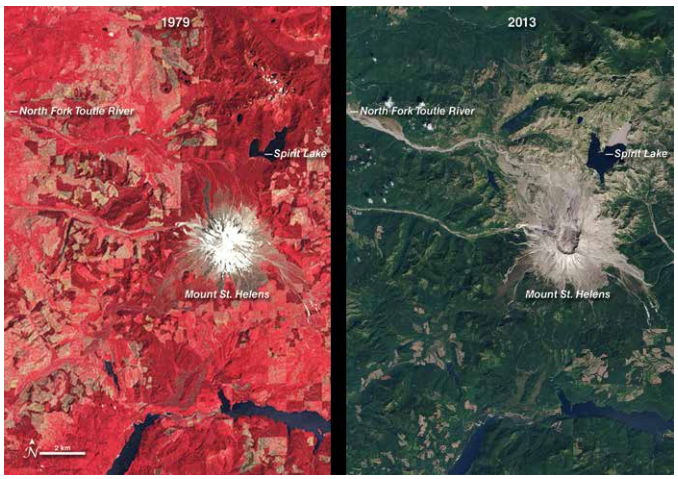

Devastation and Recovery at Mt. St. Helens

In the three decades since the eruption (1980), Mt. St. Helens has given scientists an unprecedented opportunity to witness the steps through which life reclaims a devastated landscape. The scale of the eruption and the beginning of reclamation in the Mt. St. Helens blast zone are documented in this series of images between 1979 and 2010. The older images are false-color (vegetation is red).

Not surprisingly, the first noticeable recovery (late 1980s) takes place in the northwestern quadrant of the blast zone, farthest from the volcano. It is another decade (late 1990s) before the terrain east of Spirit Lake is considerably greener. By the end of the series, the only area (beyond the slopes of the mountain itself) that remains conspicuously bare at the scale of these images is the Pumice Plain.

earthobservatory.nasa.gov/Features/WorldOfChange/sthelens.php

Amazon Deforestation

The state of Rondônia in western Brazil has become one of the most deforested parts of the Amazon. This image series, created with data from the Moderate Resolution Imaging Spectroradiometer (MODIS) onboard NASA's Terra satellite, shows the region from 2000 to 2010. By the year 2000, the frontier had reached the remote northwest corner of Rondônia. Intact forest is deep green, while cleared areas are tan (bare ground) or light green (crops, pastures). Deforestation follows a predictable pattern in these images. The first clearings appear in a fishbone pattern, arrayed along the edges of roads. Over time, the fishbones collapse into a mixture of forest remnants, cleared areas, and settlements. This pattern is common in the Amazon. Legal and illegal roads penetrate a remote part of the forest, and small farmers migrate to the area. They claim land along the road and clear some of it for crops. Within a few years, heavy rains and erosion deplete the soil, and crop yields fall. Farmers then convert the degraded land to cattle pasture, and clear more forest for crops.

earthobservatory.nasa.gov/Features/WorldOfChange/deforestation.php

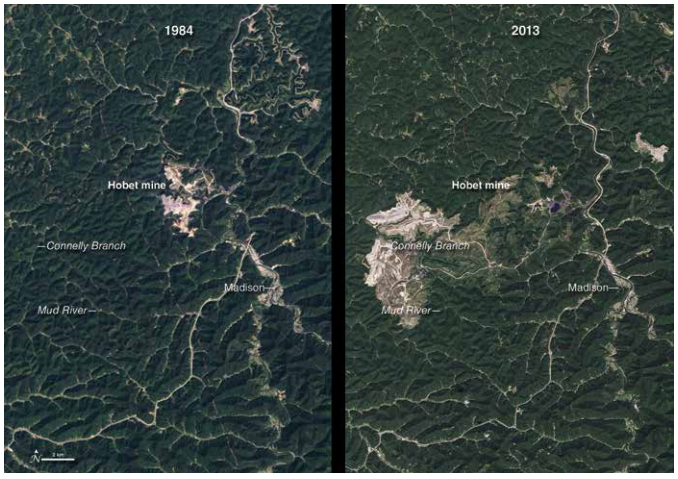

Mountaintop Mining, West Virginia

These images illustrate the growth of the Hobet mine in Boone County, WV as it moves from ridge to ridge between 1984 and 2012. The natural forested landscape appears dark green, creased by steams and indented by hollows. Active mining areas however, appear off-white and areas being reclaimed with vegetation appear light green. The law requires coal operators to restore the land to its approximate original shape, but the rock debris generally can't be securely piled as high or graded as steeply as the original mountaintop. There is always too much rock left over, and coal companies dispose of it by building valley fills in hollows, gullies, and streams. The most dramatic valley fill that appears in this series of images is what appears to be the near-complete filling of Connelly Branch from its source to its mouth at the Mud River between 1998 and 2002. Over the 28-year period, the disturbed area grew to more than 10,000 acres (15.6 square miles). While the image from 2012 shows apparent green-up of restored lands, it also shows expanded operations in the southwest and northeast. The resulting impacts to stream biodiversity, forest health, and ground-water quality are high, and may be irreversible.

earthobservatory.nasa.gov/Features/WorldOfChange/hobet.php

Forests and Biodiversity

Athabasca Oil Sands

Buried under Canada's boreal forest is one of the world's largest reserves of oil. Bitumen—a very thick and heavy form of oil (also called asphalt)—coats grains of sand and other minerals in a deposit that covers about 142,200 square kilometers of northwest Alberta.

Only 20 percent of the oil sands lie near the surface where they can easily be mined. The rest of the oil sands are buried more than 75 meters below ground and are extracted by injecting hot water into a well that liquefies the oil for pumping. This series of images from the Landsat satellite shows the growth of surface mines over the Athabasca oil sands between 1984 and 2011.

These images show slow growth between 1984 and 2000, followed by a decade of more rapid development. The first mine (from 1967, now part of the Millennium Mine) is visible near the Athabasca River in the 1984 image. The only new development visible between 1984 and 2000 is the Mildred Lake Mine (west of the river), which began production in 1996.

earthobservatory.nasa.gov/Features/WorldOfChange/athabasca.php

Human Footprints

Earth at Night

One way to study the spatial distribution, or arrangement, of human settlements is to view the planet from space during nighttime hours. The brightest areas are generally the most urbanized but not necessarily the most populated. The Visible Infrared Imaging Radiometer Suite (VIIRS) "day-night band" onboard the Suomi National Polar-orbiting Partnership (NPP) satellite can observe dim signals such as city lights, wildfires, gas flares, auroras, and reflected moonlight during nighttime hours. Swaths of data are processed to find moonless, non-cloudy picture elements, or pixels. Over time, all moonless and non-cloudy pixels for a particular location during night-time hours are averaged to produce a global image that depicts the Earth's lights at night. The data are used to study settlement patterns and the effects of future population growth. Once other sources of light like fire and lightning are removed, the "human footprint" is revealed. The remaining light comes from stable light sources such as streetlights, headlights, store signs, etc. Areas with more of these stable light sources are usually more economically developed. The image shown here is a composite of data acquired over nine days in April and thirteen days in October 2012.

earthobservatory.nasa.gov/NaturalHazards/view.php?id=79765

Shrinking Aral Sea

The Aral Sea was once the fourth largest lake in the world. In the 1960s however, the Soviet Union undertook a major water diversion project on the arid plains of Kazakhstan, Uzbekistan, and Turkmenistan, diverting the rivers that once fed the Aral Sea. Irrigation transformed desert into farmland, but devastated the sea. This animation shows the visible changes across the region from 2000 to 2013.

At the start of the series in 2000, the lake was already a fraction of its 1960 extent. The Northern Aral Sea (small) had separated from the Southern Aral Sea (large). The Southern Aral Sea had split into an eastern and a western lobe that remained tenuously connected at both ends. By 2001, the southern connection had been severed, and the shallower eastern part retreated rapidly over the next several years. After Kazakhstan built a dam between the northern and southern parts of the Aral Sea, all of the water flowing into the desert basin from the Syr Darya stayed in the Northern Aral Sea. The differences in water color are due to changes in sediment.

earthobservatory.nasa.gov/Features/WorldOfChange/aral_sea.php

Urbanization of Dubai

To expand the possibilities for beachfront tourist development, Dubai, undertook a massive engineering project to create hundreds of artificial islands along its Persian Gulf coastline. This image series shows the progress of the Palm Jumeirah Island from 2000 to 2011.

In these false-color images, bare ground appears brown, vegetation appears red, water appears dark blue, and buildings and paved surfaces appear light blue or gray. The first image shows the area prior to the island's construction. The final image, acquired in February 2011, shows vegetation on most of the palm fronds, and numerous buildings on the tree trunk. As the years pass, urbanization spreads, and the final image shows the area almost entirely filled by roads, buildings, and irrigated land.

earthobservatory.nasa.gov/Features/WorldOfChange/dubai.php

Human Footprints

Yellow River Delta

China's Yellow River is the most sediment-filled river on Earth. The river crosses a plateau blanketed with up to 300 meters (980 feet) of fine, wind-blown soil. The soil is easily eroded, and millions of tons of it are carried away by the river every year. Some of it reaches the river's mouth, where it builds and rebuilds the delta.

The Yellow River Delta has wandered up and down several hundred kilometers of coastline over the past two thousand years. Since the mid-nineteenth century, however, the lower reaches of the river and the delta have been extensively engineered to control flooding and to protect coastal development. This sequence of natural-color images shows the delta near the present river mouth at five-year intervals from 1989 to 2009. In 1996, engineers blocked the main channel and forced the river to veer northeast. By 1999, a new peninsula had formed to the north. The new peninsula thickened in the next five-years, and what appears to be aquaculture (dark-colored rectangles) expanded significantly in areas south of the river as of 2004. By 2009, the shoreline northwest of the new river mouth had filled in considerably. The land northwest of the newly fortified shoreline is home to an extensive field of oil and gas wells.

earthobservatory.nasa.gov/Features/WorldOfChange/yellow_river.php

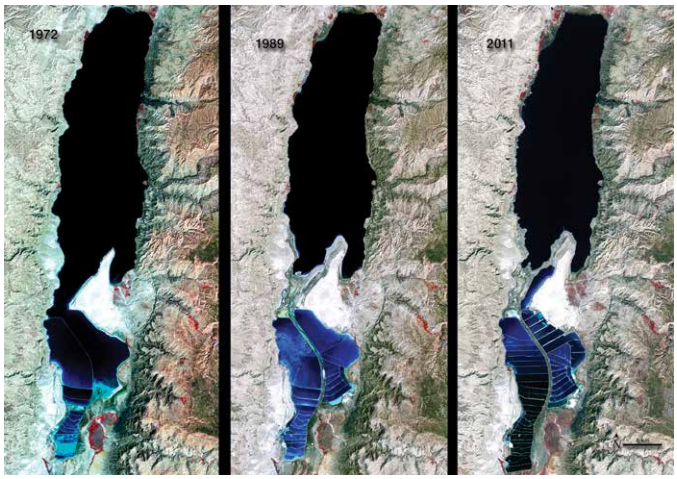

Dead Sea Salt Farming

The Dead Sea is so named because its high salinity discourages the growth of fish, plants, and other wildlife. It is the lowest surface feature on Earth, sitting roughly 1300 feet (396 meters) below sea level. On a hot, dry summer day, the water level can drop as much as one inch because of evaporation.

These three false-color images were captured in 1972, 1989, and 2011 by Landsat satellites. Deep waters are blue or dark blue, while brighter blues indicate shallow waters or salt ponds. Green indicates sparsely vegetated lands. Denser vegetation appears bright red.

The ancient Egyptians used salts from the Dead Sea for mummification, fertilizers, and potash (a potassium-based salt). In the modern age, sodium chloride and potassium salts culled from the sea are used for water conditioning, road de-icing, and the manufacturing of polyvinyl chloride (PVC) plastics. The expansions of massive salt evaporation projects are clearly visible over the span of 39 years.

earthobservatory.nasa.gov/IOTD/view.php?id=77592

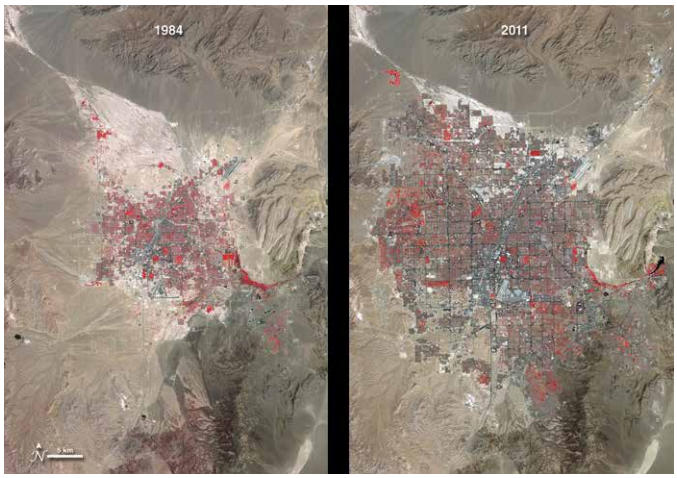

Las Vegas Urban Sprawl

The city of Las Vegas—meaning the meadows—was established in 1905. Its grassy meadows and artesian springs attracted settlers traveling across the arid Desert Southwest in the early 1800s. In the 1930s, gambling became legalized and construction of the Hoover Dam began, resulting in the cities first growth spurt. Since then, Las Vegas has not stopped growing. Population has reached nearly two million over the past decade, becoming one of the fastest growing metropolitan areas in the world. These false-color images show the rapid urbanization of Las Vegas between 1984 and 2011. The city streets and other impervious surfaces appear gray, while irrigated vegetation appears red. Over the years, the expansion of irrigated vegetation (e.g., lawns and golf courses) has stretched the city's desert bounds.

svs.gsfc.nasa.gov/goto?10721

Human Footprints

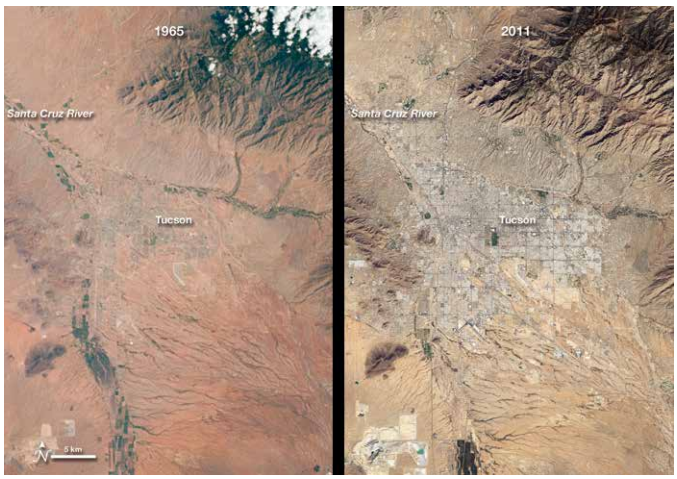

Urban Growth in Tucson, Arizona

The astronauts who snapped photos of Earth during the Mercury and Gemini missions produced more than just pretty pictures. They planted seeds at the USGS and NASA. In the mid-1960s, the director of USGS proposed a satellite program to observe our planet from above, and later described Landsat as "a direct result of the demonstrated utility of the Mercury and Gemini orbital photography to Earth resource studies."

On a flight in late August 1965, Gemini V astronauts Gordon Cooper and Pete Conrad took photos of the Earth, including a shot showing Tucson, Arizona. A lot changed in the 46 years between that photo and the satellite image acquired in 2011 by the Thematic Mapper on Landsat 5.

A comparison of the images shows more city and less green. The expansion of urbanized areas is readily identifiable by the grid pattern of city streets. Between 1965 and 2011, Tucson's population grew rapidly. In 1970, the population was 262,933; in 2010, it was 520,116.

earthobservatory.nasa.gov/IOTD/view.php?id=78613

NOTES

U.S. CENTER 2014 LIMA

Hyperwall Science Stories

svs.gsfc.nasa.gov/hw

National Aeronautics and Space Administration

www.nasa.gov

11/2014